mathematics

MDPI

Article

A Conditioned Probabilistic Method for the Solution of the Inverse Acoustic Scattering Problem

Antonios Charalambopoulos [1,*], Leonidas Gergidis [2] and Eleftheria Vassilopoulou [1]

1 Department of Mathematics, School of Applied Mathematical and Physical Sciences, National Technical University of Athens, Zografou Campus, 15780 Athens, Greece; eleftheriavassilopoulou@mail.ntua.gr
2 Department of Materials Science and Engineering, University of Ioannina, 45110 Ioannina, Greece; lgergidis@gmail.com
* Correspondence: acharala@math.ntua.gr

Abstract: In the present work, a novel stochastic method has been developed and investigated in order to face the time-reduced inverse scattering problem, governed by the Helmholtz equation, outside connected or disconnected obstacles supporting boundary conditions of Dirichlet type. On the basis of the stochastic analysis, a series of efficient and alternative stochastic representations of the scattering field have been constructed. These novel representations constitute conceptually the probabilistic analogue of the well known deterministic integral representations involving the famous Green's functions, and so merit special importance. Their advantage lies in their intrinsic probabilistic nature, allowing to solve the direct and inverse scattering problem in the realm of local methods, which are strongly preferable in comparison with the traditional global ones. The aforementioned locality reflects the ability to handle the scattering field only in small bounded portions of the scattering medium by monitoring suitable stochastic processes, confined in narrow sub-regions where data are available. Especially in the realm of the inverse scattering problem, two different schemes are proposed facing reconstruction from the far field and near field data, respectively. The crucial characteristic of the inversion is that the reconstruction is fulfilled through stochastic experiments, taking place in the interior of conical regions whose base belong to the data region, while their vertices detect appropriately the supporting surfaces of the sought scatterers.

Keywords: wave scattering; Helmholtz equation; inverse problems; stochastic differential equations

MSC: 35J05; 35J25; 60H10; 78A46

Citation: Charalambopoulos, A.; Gergidis, L.; Vassilopoulou, E. A Conditioned Probabilistic Method for the Solution of the Inverse Acoustic Scattering Problem. *Mathematics* **2022**, *10*, 1383. https://doi.org/10.3390/math10091383

Academic Editor: Nikolaos Tsitsas

Received: 23 March 2022
Accepted: 18 April 2022
Published: 20 April 2022

1. Introduction

In contrast to the traditional global methods, local methods give the solution of a partial differential equation at an arbitrary point of its domain directly, instead of extracting the response value at this point from the whole field solution. These methods are based on probabilistic interpretations of certain partial differential equations. The relationship between stochastic processes and parabolic and elliptic differential equations was demonstrated a long time ago by Lord Rayleigh [1] and Courant [2], respectively. The development of the probabilistic methods is based on the Itô calculus, properties of Itô diffusion processes, and Monte Carlo simulations. The theoretical considerations supporting the probabilistic methods involve random processes and stochastic integrals. An elaborate presentation of this framework can be found in [3–6] and the references cited therein. The main idea of these approaches concerns boundary value problems in bounded domains: A probabilistic manner to interpret the value of the solution of the boundary value problem at a specific point x is to consider a plethora of stochastic trajectories, emanating from x and driven by a drift and diffused by a Wiener process connected both directly with the coefficients of the differential operator under investigation. These trajectories travel inside the bounded domain and cross the boundary in finite time. Averaging the values of the field at the boundary hitting points (thus evoking the boundary condition of the problem) gives a very good estimation of the sought solution of the boundary value problem. In exterior domains, the situation changes drastically since the unboundedness of the domain does not provide any reason justifying the aforementioned boundary hitting in finite time. This is the main reason why no systematic probabilistic attempts had been made to face boundary value problems in unbounded domains.

Recently, the probabilistic interpretation of boundary value problems in exterior domains has been reestablished appropriately in [7]. The main effort in that work was to force the trajectories emanating from the point x and travelling inside the infinite domain D to hit the boundary ∂D in finite time. Without special treatment, the generated trajectories have a strong probability to travel to infinity without hitting the boundary of the domain. Actually, even if some paths cross the boundary, their travel time could be very large, creating strong difficulties to the application of the Monte Carlo simulation. The monitoring of the trajectories is accomplished by selecting appropriately a set of attracting or repulsive points ξ, which constitute irregular points for the stochastic process. This actually is not enough since the orientation of the trajectories towards or away from these singular points is simultaneously guaranteed by the repulsive lateral surfaces of several cones $\mathcal{K}$ having as vertexes the singular points. These cones are repulsive since on the lateral surfaces the driving terms of the stochastic processes obtain infinite values. The process of the directivity of the stochastic paths inside the cones under discussion has been presented extensively in [7] but we focus here on the fact that the monitoring of the curves is mainly accomplished via suitable stochastic differential equations with driving terms generated by the eigen-solutions of the Laplace operator in local (associated to the cones) spherical coordinates. The point is that under this directionality, the generated trajectories hit (for the first time) the boundary ∂D in finite time. All these paths are gathered and exploited as follows: The points of the boundary on which the first exit occurs—the traces of the trajectories on the boundary—are selected and offer a set of points on which the average of the values of the boundary data of the boundary value problem is calculated thus formatting a first accumulation term. In addition, on every trajectory a stochastic integral is calculated where the integrand is the inhomogeneous term of the underlying differential equation. The mean value of these integrals over the large number of trajectories forms a second accumulator which is superposed to the first one, (this second term is absent in the case of a homogeneous differential equation) leading to the construction of an extended mean value term. When the number of the trajectories increases, the aforementioned total mean value converges to the corresponding probabilistic expectation value of the underlying fields, which in turn coincides with the value sought from the beginning of the solution of the boundary value problem at the starting point x. The description above refers rather to the Dirichlet problem, which is the main subject of investigation in the present work but similar arguments are encountered in the Neumann boundary value problem [8,9]. One of the main advantages of the probabilistic approach is that it is based on very stable and accurate Monte Carlo simulations. In [7], the above methodology has been developed and applied mainly in the exterior Laplace boundary value problem, referring so to potential functions.

In the present work, a probabilistic framework handling the acoustic scattering problem is developed. More precisely, we consider the exterior Dirichlet boundary value problem involving the Helmholtz operator, without restriction on the wavenumber. It worth mentioning that working with stochastic trajectories that stemmed from the Helmholtz equation itself diversifies qualitatively the stochastic framework by offering two alternative stochastic differential regimes, referring to preselected outgoing or ingoing wave propagation. In brief terms, this deviation is due to the nature of the driving terms which govern, in conjunction with the Wiener process, the topology of the stochastic curves. These driving terms are built in the form $\frac{\nabla h}{h}$—where h belongs to the kernel of the Helmholtz operator—and are responsible for the probabilistic conditioning. They are expressed in terms of spherical local coordinates inside the cones $\mathcal{K}$. The crucial remark is that two alternatives emerge: When the generating function is selected to be equal to $h = h_m = y_m(kr)P_m(\cos\theta)$, where y_m stands for the spherical Bessel function of second kind and order m, the trajectories are forced to move inwardly, from the observation point towards the scatterer's region. This behavior is reminiscent of the stochastic design encountered in [7]. In contrast to that, when the selection is set to $h_m = j_m(kr)P_m(\cos\theta)$, involving now the spherical Bessel functions of first kind $j_m(kr)$, the stochastic curves present an opposite behavior. More precisely, most of the trajectories emanating from x move fast away outwards, hitting the exterior cup of the cone, which represents a portion of the measurement region located at the near field or far field regime, depending on the measurement status and the subsequent narrowness (the angle of the cone is just the first positive root of the Legendre polynomial $P_m(\cos\theta)$) of the cone. The two situations above can be melted by selecting the radial part of the driving function h_m to be a combination of the spherical Bessel functions: $C_m j_m(kr) - y_m(kr)$. Choosing suitably the coefficient C_m, it is feasible to settle a stochastic framework assuring equipartition of stochastic experiments in two directions: The outgoing trajectories hitting the measurement region and revealing the contribution of the data and the ingoing trajectories hitting the scatterer and activating the boundary condition. This is an efficient manner to acquire a stochastic representation for the acoustic field u at the observation point x, which constitutes simultaneously the emanation point of the stochastic experiments. Actually, the description above settles the framework of the direct scattering problem.

In the realm of the inverse scattering problem, which is the cornerstone of the current work, the common issue with the settlement above is the invocation of the radial function $C_m j_m(kr) - y_m(kr)$, establishing the aforementioned equipartition of the stochastic experiments. The essential structural difference stems from the simple argument that a representation scheme involving three separate terms (the value of the acoustic field u at the starting point x and the expectation values of the field on both detached portions of the cone with the scatterer and the data region) is an underdetermined scheme. To diminish the unknowns of the problem, we do not apply the stochastic analysis to the acoustic field $u(X)$ itself, but to the solenoidal vector Helmholtz equation solution $M(X;x) = (X - x) \times \nabla u(X)$ and potentially to the scalar Helmholtz equation solution $(X - x) \cdot \nabla \times M(X;x)$. These functions merit the principal property of vanishing at the starting point x, leaving alone among the terms of the aforementioned triple, the tag of war between the expectation values over the data region and the scatterer's surface, where the boundary condition prevails. Following a sampling process, in the case that the vertex of the cone detects the scatterer's surface points, a functional measuring the balance between the abovementioned measurement term and the boundary condition attains minimum values and quantifies the inversion.

The structure of the work is developed as follows: In Section 2, the mathematical principles of the scattering problem are briefly presented. In Section 3, the stochastic differential equations that stemmed from the boundary value problem under discussion are constructed and the suitably layered conical regions serving as the domains of the stochastic processes are confined. The probabilistic analysis of the subsequent stochastic differential system is also developed. This analysis focuses on the analytical investigation of a priori estimates concerning all the involved probabilities of hitting the several surface portions of the conical structures. Especially in Section 3.2, three separate stochastic representations of the scattered field are provided based on outgoing, ingoing and mixed-type propagating stochastic trajectories. Special attention has been paid to the third case constituting a stochastic representation, embodying, in an equipartitioned manner, the contribution of the data region as well as of the scatterer's surface. These representations and mainly the third one constitute alternative probabilistic representations of the scattered field and could be considered as the stochastic analogue of the well known classical integral representations, produced on the basis of Green's theorem. In Section 4, some crucial parameters of the stochastic implementation are investigated as far as their numerical implementation is concerned. The solution of the inverse scattering problem from convex scatterers on the basis of exploiting stochastically far field data and the stochastic process of transferring data from the far field to the near field region are presented in Section 5. The analytic as well as numerical investigation are extensively provided and testified to via interesting special cases. In Section 6, the inverse reconstruction algorithm in the case of exploitation of near data is implemented and applied in connected and disconnected scatterers.

2. Helmholtz Equation and Scattering Processes

Let us consider an open bounded region D in $\mathbb{R}^3$, confined by a smooth (with continuous curvature to support the classical version of the probabilistic calculus, though there exist improvements allowing Lipschitz domains [10]) surface ∂D, standing for a hosted inclusion inside the surrounding medium $D^e = R^3 \backslash \bar{D}$.

The elliptic boundary value problem representing acoustic scattering of time harmonic stationary waves by obstacles is the one involving the Helmholtz equation, which is produced after imposing time harmonic dependence in wave equation. So, the acoustic scattering field $u(x)\exp(-i\omega t)$ emanated from the interference of an incident time harmonic wave $u^{in}(x,t) = \exp(i(k\hat{k}\cdot x - \omega t))$ with the soft scatterer $\bar{D} \subset R^n$ satisfying the following boundary value problem

$$(\Delta + k^2)u(x) = 0, \quad x \in D^e \tag{1}$$

$$u(x) = -\exp(ik\hat{k}\cdot x), \quad x \in \partial D \tag{2}$$

$$\lim_{r\to\infty} r^{-1}\left(\frac{\partial u(x)}{\partial r} - iku(x)\right) = 0, \tag{3}$$

where we recognize the wave number $k \neq 0$, the unit vector $\hat{k}$, indicating the direction of the incident wave, and the angular frequency ω of the scattering process. Sommerfeld radiation Condition (3), which holds uniformly over all possible directions $\hat{x} = \frac{x}{r}$, assures that the scattered field is an outgoing field. Indeed, this condition not only gives information about the asymptotic behavior of the scattered wave but also incorporates the physical property according to which the whole energy of the scattered wave travels outwards, leaving behind the scatterer from which it emanates. In the case of a hard scatterer, Dirichlet boundary Condition (2) should be replaced by the Neumann boundary condition. In that case, we have knowledge about the normal derivative of the field $\frac{\partial u}{\partial n}$ on the surface ∂D. In any case, it is well known that asymptotically it holds that

$$u(x) = \frac{e^{ik|x|}}{|x|} u_\infty(\hat{x};\hat{k},k) + u_1(x), \;\; |x|u_1(x) \to 0, \text{ as } \; |x| \to \infty \tag{4}$$

where we recognize the far field pattern, or, alternatively stated, scattering amplitude $u_\infty(\hat{x};\hat{k},k)$, totally characterizing the behavior of the wave field $u(x)$ several wave-lengths away from the scatterer D. Actually, Equation (4) offers the first term of the asymptotic expansion of $u(x)$ via the famous Atkinson–Wilcox expansion theorem [11]. This theorem establishes a recurrence relation between the participants of this expansion. All but the first term are incorporated in the remaining field $u_1(x)$. A more systematic treatment of this expansion is sometimes needed and the current work offers such an opportunity as the implication of this stuff is needed in Remark 2 of Section 5.

In all cases, the direct exterior boundary value problem consists in the determination of the field $u(x)$ outside D when boundary data (i.e., the function $f(x) = -\exp(ik\hat{k}\cdot x)$) and geometry (i.e., the shape of ∂D) are given. In fact, in most applications, we are interested in determining the remote pattern of this field far away from the bounded domain D. For example, in the case of the Dirichlet BVP (1)–(3), it would be sufficient to determine the far field pattern $u_\infty(\hat{x};\hat{k})$ participating in the representation (4) if we deal with an application in which we do not have access near the domain D.

The inverse exterior boundary value problem aims at determining the shape of the surface ∂D when the boundary data is known and the remote pattern is measured. Equivalently, instead of considering as data the measured remote field, it is usual to have at hand the Dirichlet to Neumann (DtN) operator on a sphere—or part of it—surrounding the domain D and the scattered field on it. Generally, a large class of interesting inverse boundary value problems are based on data incorporating both the measured field along with its normal derivative on a given surface belonging to the near field region (Pertaining to the Helmholtz operator, we refer to [12] (Section 3.2) as an excellent reference relevant to the construction of the DtN mapping). It is known [13] that a specific scattering amplitude (far field pattern) leads to a unique DtN oparator, providing parallel pace to those approaches. On the other hand, the involvement of the Dirichlet to Neumann (DtN) operator is valuable but generally intricate, given that in principle this operator is not local. The present work aims as a supplementary to offer, as a byproduct, a localization concept to the reduction of the DtN operator from the far field pattern. This localization is in the core of the nature of locality supported by the implication of probabilistic methods in the solvability of boundary value problems.

3. The Stochastic Differential Equations in Connection with the Scattering Problem

In the core of the present work lie the stochastic differential equations of the type

$$dX_t = b(X_t)dt + \sigma(X_t)dB_t, \quad 0 \leq t \leq T, \;\; X_0 = x. \tag{5}$$

In the equation above, $T > 0$, while $b(.) : \mathbb{R}^n \to \mathbb{R}^n$ and $\sigma(.) : \mathbb{R}^n \to \mathbb{R}^{n\times n}$ are measurable functions. The Brownian motion B_t is n-dimensional while the initial state x is fixed. It is proved in [4] that, under certain conditions on b and σ, the stochastic differential Equation (5) has a unique t-continuous solution X_t (Itô diffusion) which is adapted to the filtration (increasing family) $\mathcal{F}_t$ generated by $B_s; s \leq t$. In addition $E[\int_0^T |X_t|^2 dt < \infty]$. We may integrate obtaining

$$X_t = x + \int_0^t b(X_s)ds + \int_0^t \sigma(X_s)dB_s, \;\; 0 \leq t \leq T, \tag{6}$$

where we recognize [4] the Itô integral $\int_0^T \sigma(X_t)dB_t$. The specific conditions mentioned above impose at most linear growth and Lipschitz behavior of the coefficients, uniformly over time.

The unique solution X_t, generated by the arguments above, is called the *strong* solution, because the version B_t of the Brownian motion is given in advance and the solution constructed from it is $\mathcal{F}_t$-adapted. The price we pay to obtain such a good and unique solution is the restriction on the coefficients b and σ. In general terms, the linear growth excludes the appearance of explosive solutions while the Lipschitz condition establishes uniqueness.

The coefficient $b(X_t)$ is known as the drift of the process. In the absence of the random term, the drift is exclusively responsible for the evolution of the dynamical system X_t and so "drives" the vector X_t. It clearly retains this basic property in the case of small randomness, induced by small $\sigma(X_t)$, and the trajectory of the process keeps its orientation, while obtaining a fluctuating morphology due of course to the randomness. It is an issue of great importance to investigate the behavior of composite functions of the form $F(t,\omega) = f(t, X_t) = f(t, X(t))$, where $f(t,x) = (f_1(t,x), f_2(t,x), ..., f_p(t,x))$ is a C^2 map from $[0,\infty) \times \mathbb{R}^n$ into $\mathbb{R}^p$ and ω here denotes an arbitrary element of the probability set Ω participating in the triple $(\Omega, \mathcal{F}, P)$ defining the probability space. The method for this effort is provided by the well known multi-dimensional Itô formula, according to which $F(t,\omega)$ is again an Itô process with components F_k, $k = 1,2,...,p$, satisfying

$$dF = \frac{\partial F}{\partial t}(t,X)dt + \sum_i \frac{\partial F}{\partial x_i}(t,X)dX_i + \frac{1}{2}\sum_{i,j} \frac{\partial^2 F}{\partial x_i \partial x_j}(t,X)dX_i dX_j, \tag{7}$$

where the relations $dB_i dB_j = \delta_{ij}dt$, $dB_i dt = dt dB_i = 0$ span the calculus of products between infinitesimals. We evoke here $E^x(Y_t)$, the well known [4] expectation of a stochastic process Y_t where the superscript is necessary to indicate the starting point of the involved stochastic processes.

For every Itô diffusion X_t in $\mathbb{R}^n$, the infinitesimal *generator* A is defined by $Af(x) = lim_{t\downarrow 0}\frac{E^x[f(X_t)]-f(x)}{t},\ x \in \mathbb{R}^n$. This limit is considered in the point-wise classical sense. For every x, the set $D_A(x)$ is defined as the set of all the functions f, guaranteeing the existence of the limit. In addition D_A denotes the set of functions assuring the existence of the limit for all $x \in \mathbb{R}^n$. The domain D_A incorporates $C_0^2(\mathbb{R}^n)$. More precisely, every $f \in C_0^2(\mathbb{R}^n)$ belongs to D_A and satisfies

$$Af(x) = \sum_i b_i(x)\frac{\partial f}{\partial x_i} + \frac{1}{2}\sum_{i,j}(\sigma\sigma^T)_{i,j}(x)\frac{\partial^2 f}{\partial x_i \partial x_j}. \tag{8}$$

The infinitesimal generator offers the link between the stochastic processes and the partial differential equations.

The well known Dynkin's formula [4] connects the infinitesimal operator A with expectation values of suitable stochastic processes. Indeed, let $f \in C_0^2(\mathbb{R}^n)$ and suppose that τ is a stopping time (i.e., $\{\omega : \tau(\omega) \leq t\} \in \mathcal{F}_t,$ for all $t \geq 0$) with $E^x[\tau] < \infty$. Then

$$E^x[f(X_\tau)] = f(x) + E^x\left[\int_0^\tau Af(X_s)ds\right]. \tag{9}$$

The existence of a compact support for the functions f is not necessary if τ is the first exit time of a bounded set. Dynkin's formula is very helpful in obtaining stochastic representations of boundary value problem solutions in bounded domains. As for example, the C^2- solution of the harmonic Dirichlet boundary value problem (with surface data ϕ) inside a bounded domain D in $\mathbb{R}^n$:

$$\begin{aligned} &\Delta u(x) = 0,\ x \in D \\ &u(x) = \phi(x),\ x \in \partial D, \end{aligned}$$

has the stochastic representation

$$u(x) = E^x[\phi(B_{\tau_D})], \tag{10}$$

as an immediate consequence of Equation (9) with $b = 0, \sigma_{i,j} = \delta_{i,j}$ (and so $X_t = B_t$ and $A = \frac{1}{2}\Delta$). In the stochastic framework under discussion, the first exit time τ_D from the open set D is a particular type of stopping times and plays a special role. At that time, the stochastic process X_t, obeying Equation (5) with $X_0 = x$ and very large T, "hits" the boundary ∂D. This particular exit process brings into light the boundary itself and a crucial connection is established between the solution of the differential equation and the points of the boundary on which data are given. Generally the process B_t represents points in $\mathbb{R}^n$, but more precisely, the multidimensional stochastic field B_{τ_D} represents points on the surface ∂D.

It is clear that the situation changes drastically when we are treating the corresponding exterior harmonic boundary value problem defined on the unbounded open domain $D^e := R^n \backslash \bar{D}$. We focus on the Helmholtz equation $(\Delta + k^2)u = 0$, governing the behavior of the scattered field u. According to the aforementioned discussion, the first idea to represent stochastically the problem might be to adopt the genuine Brownian motion again, with infinitesimal generator $A = \frac{1}{2}\Delta$ helping in adapting Dynkin's formula as follows:

$$\begin{aligned} &E^x[u(X_\tau)] = E^x[u(B_\tau)] = u(x) + E^x\left[\int_0^\tau Au(B_s)ds\right] \Rightarrow \\ &u(x) = E^x[u(B_\tau)] + \frac{k^2}{2}E^x\left[\int_0^\tau u(B_s)ds\right], \end{aligned} \tag{11}$$

where τ now is the first time of exit from the set D^e. Unfortunately, this representation is not adequate any more. Indeed, the Brownian motion in $\mathbb{R}^3$ is transient, which means that $P^x(\tau < \infty) < 1$ and then the prerequisite (for the validity of Dynkin's formula) of almost surely finite flying time (before hitting for first time the boundary of D^e) of the process B_t is not guaranteed. The violation of the finite life time could be avoided if a more general form of Dynkin's rule was used ($\mathcal{X}_A$ stands for the characteristic function of the set A) :

$$u(x) = E^x[u(B_\tau)\mathcal{X}_{\{\tau<\infty\}}] + \frac{k^2}{2}E^x\left[\int_0^\tau u(B_s)ds\right]. \tag{12}$$

However, the validity of this formula requires that $E^x\left[\int_0^\tau |u(B_s)|ds\right] < \infty$, which is strongly ambiguous since u has no compact support and the life time variable is not controllable. In addition, the Monte Carlo simulation would be very slow since a part of trajectories could ramble for a long time before hitting the boundary or just making eternal loops inside the exterior space D^e. Even if these drawbacks were bypassed, the implication of the integral term is not desirable since it involves the values of the field along several paths and actually necessitates the enrichment of data over a large part of the exterior space, a fact which is unrealizable. The information is restricted on the surface of the scatterer (boundary condition) and on the data surface where measurements are gathered.

As discussed in the Introduction, for theoretical and application reasons, it is necessary to impose a driving mechanism forcing the trajectories to have finite life time and to obtain exploitable directivity towards the regions of given information. The initiative concept is to select a point ξ inside the bounded component D. Placing this auxiliary point inside or outside D depends on two different states of probabilistic conditioning as presented in [7]. In the present work focusing on the inverse problem, the first choice is adopted. This point could be the coordinate origin O or could be selected according to the specific features of the problem. Let $x \in D^e$ be once again the initial point of the stochastic process under construction. We consider the unit vector $\hat{n}_{x,\xi} := \frac{x-\xi}{|x-\xi|} = \frac{y}{|y|}$. For simplicity we denote $\hat{n}_{x,\xi}$ as $\hat{n}$ since the points x, ξ are assumed as fixed parameters, though the same procedure might be profitable to be applied for several pairs (x, ξ). We introduce now two sets of functions belonging to the kernel of the Helmholtz operator. More precisely, evoking the well known Legendre polynomial functions (It is essential to select the normalization condition $P_m(1) = 1$) $P_m(\cos\theta), \theta \in [0, \pi]$ and the spherical Bessel (j_m) and Neumann (y_m) functions, we introduce two families ($l = 1, 2$) of eigensolutions: $h_{m,l}(y; k) = P_m(\hat{n} \cdot y/|y|)\mathcal{Q}_{m,l}(k|y|)$, $m = 0, 1, 2, ...$, where $\mathcal{Q}_{m,1}(k|y|) = j_m(k|y|)$ and $\mathcal{Q}_{m,2}(k|y|) = y_m(k|y|)$. For simplicity, we suppress the dependence on the wavenumber, denoting $h_{m,l}(y) = h_{m,l}(y; k)$.

Every member $h_{m,l}(y)$, $m = 0, 1, 2, ...$ of the l-family gives birth to a different stochastic process X_t, Y_t where $X_t = Y_t + \xi$, which obeys the stochastic rule

$$dY_t = \frac{\nabla h_{m,l}(Y_t)}{h_{m,l}(Y_t)}dt + dB_t, \quad 0 \le t \le T, \;\; Y_0 = x - \xi \tag{13}$$

or equivalently

$$dX_t(= dY_t) = \frac{\nabla h_{m,l}(X_t - \xi)}{h_{m,l}(X_t - \xi)}dt + dB_t, \;\; 0 \le t \le T, \;\; X_0 = x. \tag{14}$$

Both processes X_t, Y_t depend on the adopted member $h_{m,l}$ but this dependence is ignored in the symbolism of them, for simplicity. The Helmholtz equation's solution $h_{m,l}$ is expressed in local spherical coordinates adapted to the cone $\mathcal{K}_m = \xi + K_m = \xi + \{y \in R^3 : \theta \in [0, \theta_{m,1})\}$ with vertex located at ξ and axis parallel to $\hat{n}$. The pair (ξ, x) defines the z-axis of this local coordinate system. In y-terminology, the origin of the coordinates coincides with the point ξ. Finally, $\chi_{m,1} = \cos(\theta_{m,1})$ is the closest root of $P_m(\chi)$ to the right endpoint of its domain $[-1, 1]$ and is indicative of the narrowness of the cone.

We will gather here some information whose justification is postponed: Working with a particular $h_{m,l}$, the process X_t has a specific driving term $\frac{\nabla h_{m,l}}{h_{m,l}}$, which defines drastically the orientation of the trajectories. We will see in following sections that depending on the kind of the involved spherical Bessel's function, the vertex ξ is a strong attractor or repellent for the process. Furthermore, the paths are also repelled from the lateral surface of the cone $\mathcal{K}_m$ and in any case the trajectories are forbidden to cross this lateral surface. So, the process X_t is generated in $\mathcal{K}_m \cap D^e$—at the point x—and is attracted or repelled by the singularity ξ at the same time that it is repelled by the boundary $\partial\mathcal{K}_m \cap D^e$. The trajectories cannot escape the cones $\mathcal{K}_m$, which become narrower as the parameter m increases.

Before investigating the above-presented stochastic processes, it is necessary to make a concrete construction of the domain confining the mobility of the paths.

This emanates from the strict conditions required to assure the existence and uniqueness of the solution of the stochastic differential equation under examination. The coefficients of the s.d.e. (5) must be regular functions and share Lipschitz behavior, uniformly over time [4]. In our case this is accomplished only if we insert into the conical structures interior protective surfaces, thus avoiding the sets on which the driving terms become irregular. In Figure 1, we give the generic slightly modified conical region supported by a large cup and a small spherical shell deteriorating the singular point ξ as well as a specification of this region by selecting the protective interior conical surface to coincide with $\mathcal{K}_{m+\gamma}$. The regions under discussion are defined as follows: $\tilde{D}^e_{m,\epsilon}(\xi) = D^e \cap \{\xi + y : y \in R^3 \text{ with } \arccos\left(\hat{n}_{x,\xi} \cdot \frac{y}{|y|}\right) \in [0, \theta_{m,1} - \epsilon)\} \cap \{z \in \mathbb{R}^n : \eta < |z - \xi| < L\}$ and $\tilde{D}^{e,\gamma}_m(\xi) = D^e \cap \mathcal{K}_{m+\gamma} \cap \{z \in \mathbb{R}^n : \eta < |z - \xi| < L\}$ (with small positive parameters $\epsilon, \gamma << 1$). The first case is the most general selection while the second one is going to be the most profitable for the application of the methodology.

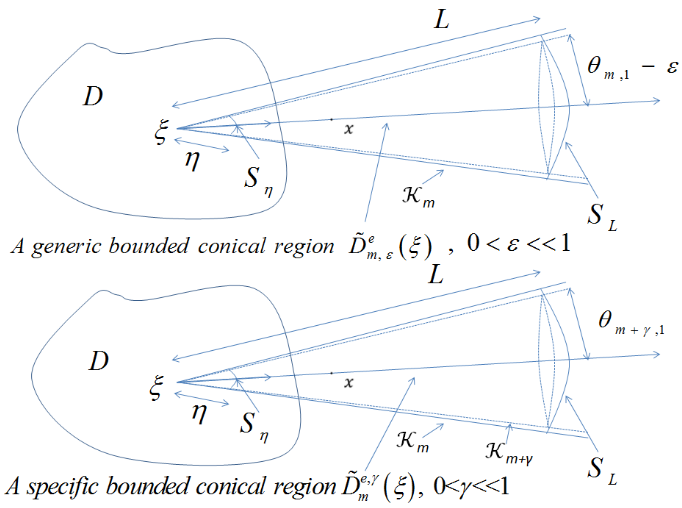

Figure 1. Inserting cups and interior conical "cushioning" to guarantee regular driving terms.

3.1. The Probabilistic Analysis of the Stochastic Differential Equations Related to the Scattering Problem

Applying Equation (13) with $h_{m,1}(Y_t) = P_m(\hat{n} \cdot Y_t/|Y_t|)\mathcal{Q}_{m,1}(k|Y_t|) = P_m(\cos(\Theta_t))j_m$ $(k|Y_t|)$ and exploiting the recurrence relation of spherical Bessel functions, we find that

$$dY_t = \mathcal{H}_m(k|Y_t|)\frac{Y_t}{|Y_t|^2}dt - \frac{\sin(\Theta_t)P'_m(\cos(\Theta_t))}{|Y_t|P_m(\cos(\Theta_t))}\hat{\Theta}_t dt + dB_t, \tag{15}$$

with

$$\mathcal{H}_m(\lambda) := \frac{\lambda j_{m-1}(\lambda)}{j_m(\lambda)} - (m+1), \ \ \lambda > 0. \tag{16}$$

This function takes the value m at $\lambda = 0$, as a simple asymptotic analysis reveals. In addition, it decreases until the first root, while positivity above a lower bound level $\delta > 0$ is guaranteed when $\lambda < e_m$, where the values $e_m(\delta)$ are uniquely determined due the monotonicity of $\mathcal{H}_m$ (see Figure 2). It is noticeable that the sequence $e_m,\ m = 0, 1, 2, ...$ increases ($e_{m+1} > e_m, \quad m = 0, 1, 2, ...$), while their specific values are very useful in the numerical treatment of the problem, as will be clarified in forthcoming sections.

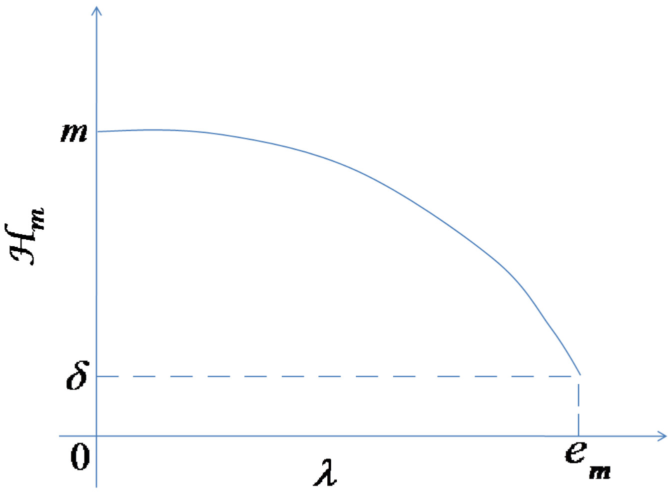

Figure 2. The decreasing positive function $\mathcal{H}_m(\lambda)$.

The parameter L, defining the height of the detached exterior space $\tilde{D}^e_{m,\epsilon}(\xi)$, is usually selected equal to the value $\frac{e_m}{k}$.
The following result concerns the duration of the stochastic process traveling inside $\tilde{D}^e_{m,\epsilon}(\xi)$.

Proposition 1. *Let the starting point x belong to $\tilde{D}^e_{m,\epsilon}(\xi)$. Then the expectation of the first exit time τ (from the detached exterior space $\tilde{D}^e_{m,\epsilon}(\xi)$) is estimated as follows:*

$$(2\delta + 3)E^x(\tau) \leq (E^x(|Y_\tau|^2) - |x - \xi|^2) \leq (2m + 3)E^x(\tau). \tag{17}$$

As a consequence,

$$E^x(\tau) \leq \frac{1}{2\delta + 3}\left(\frac{e_m^2}{k^2} - |x - \xi|^2\right). \tag{18}$$

Proof. We apply the Itô formula (see [4]) to the function $F(t, \omega) = f(Y_t(\omega)) = |Y_t(\omega)|^2$ and obtain in tensor form

$$d|Y_t|^2 = \nabla|Y_t|^2 \cdot dY_t + \frac{1}{2}\nabla\nabla|Y_t|^2 : dY_t dY_t. \tag{19}$$

We find that $\nabla|Y_t|^2 = 2Y_t$ and $\nabla\nabla|Y_t|^2 = 2I$, where I is the 3×3 identity tensor. Consequently, Equation (19) becomes

$$d|Y_t|^2 = 2(Y_t \cdot dY_t) + (dY_t \cdot dY_t). \tag{20}$$

The products $(Y_t \cdot dY_t)$ and $(dY_t \cdot dY_t)$ must be determined via the stochastic differential Equation (15) and the usual infinitesimal product relations of Itô calculus. Indeed, we obtain

$$Y_t \cdot dY_t = Y_t \cdot \left(\mathcal{H}_m(k|Y_t|)\frac{Y_t}{|Y_t|^2}dt - \frac{\sin(\Theta_t)P'_m(\cos(\Theta_t))}{|Y_t|P_m(\cos(\Theta_t))}\hat{\Theta}_t dt + dB_t\right) = \mathcal{H}_m(k|Y_t|)dt + Y_t \cdot dB_t,$$
$$dY_t \cdot dY_t = 3dt$$

Consequently,

$$d|Y_t|^2 = (2\mathcal{H}_m(k|Y_t|) + 3)dt + 2Y_t \cdot dB_t. \tag{21}$$

Integrating, taking the expectation value and exploiting the independence of Y_t, dB_t, we obtain

$$E^x(|Y_t|^2) - |x-\xi|^2 = E^x\left\{\int_0^\tau (2\mathcal{H}_m(k|Y_s|) + 3)ds\right\}. \tag{22}$$

Given that

$$\delta \leq \mathcal{H}_m(k|Y_s|) \leq m, \ \text{ for } k|Y_s| < e_m,$$

we obtain Relation (17). On the basis of the restriction $|Y_t| < \frac{e_m}{k}$, Relation (17) easily provides (18). □

One immediate consequence of the above result is that $E^x(|Y_\tau|^2) > |x-\xi|^2$. So, as expected on the basis of the repellent role of the auxiliary point ξ, the paths are mostly forced to move outwards.
One important issue concerns the probability of the trajectories approaching the lateral surface. We recall that the interior conical protective surface serving at avoiding singular behavior of the driving term is no longer impenetrable, although it retains a repelling role.

Proposition 2. *If the domain of the stochastic process (15) is $\tilde{D}^e_{m,\epsilon}(\xi)$ and τ is the first exit time from this domain, then the probability of escaping from the lateral surface, instead of the cups, converges to zero as the parameter ϵ tends to zero:*

$$\lim_{\epsilon\to 0} P^x\left(\left\{X_\tau \in \partial\tilde{D}^e_{m,\epsilon}(\xi)\right\} \cap \{\Theta_\tau = \theta_{m,1} - \epsilon\}\right) = 0. \tag{23}$$

Proof. We apply the Itô formula to the function $\frac{1}{h^\zeta_{m,1}(Y_t)}$ ($\zeta \in \mathbb{R}$), where $h_{m,1}$ satisfies the Helmholtz equation, and obtain straightforwardly that

$$d\left(\frac{1}{h^\zeta_{m,1}(Y_t)}\right) = -\zeta\frac{\nabla h_{m,1}(Y_t)}{h^{\zeta+1}_{m,1}(Y_t)} \cdot dY_t + \frac{1}{2}\left[\zeta(\zeta+1)\frac{\nabla h_{m,1}(Y_t)\nabla h_{m,1}(Y_t)}{h^{\zeta+2}_{m,1}(Y_t)} - \zeta\frac{\nabla\nabla h_{m,1}(Y_t)}{h^{\zeta+1}_{m,1}(Y_t)}\right] : dY_t dY_t \Rightarrow$$
$$d\left(\frac{1}{h^\zeta_{m,1}(Y_t)}\right) = -\zeta\frac{|\nabla h_{m,1}(Y_t)|^2}{h^{\zeta+2}_{m,1}(Y_t)}dt + \frac{1}{2}\zeta(\zeta+1)\frac{|\nabla h_{m,1}(Y_t)|^2}{h^{\zeta+2}_{m,1}(Y_t)}dt - \frac{\zeta}{2}\frac{\Delta h_{m,1}(Y_t)}{h^{\zeta+1}_{m,1}(Y_t)}dt - \frac{\zeta}{h^{\zeta+1}_{m,1}(Y_t)}\nabla h_{m,1}(Y_t) \cdot dB_t \Rightarrow$$
$$d\left(\frac{1}{h^\zeta_{m,1}(Y_t)}\right) = \frac{1}{2}\zeta(\zeta-1)\frac{|\nabla h_{m,1}(Y_t)|^2}{h^{\zeta+2}_{m,1}(Y_t)}dt + \frac{\zeta}{2}k^2\frac{1}{h^\zeta_{m,1}(Y_t)}dt - \frac{\zeta}{h^{\zeta+1}_{m,1}(Y_t)}\nabla h_{m,1}(Y_t) \cdot dB_t. \tag{24}$$

Equation (24) will be repeatedly exploited in the sequel. In the meanwhile, we select $\zeta = 1$, obtaining

$$d\left(\frac{1}{h_{m,1}(Y_t)}\right)e^{-\frac{k^2}{2}t} - \frac{k^2}{2}\frac{1}{h_{m,1}(Y_t)}e^{-\frac{k^2}{2}t}dt = -e^{-\frac{k^2}{2}t}\frac{1}{h^2_{m,1}(Y_t)}\nabla h_{m,1}(Y_t) \cdot dB_t \Rightarrow d\left(\frac{1}{h_{m,1}(Y_t)}e^{-\frac{k^2}{2}t}\right)$$
$$= -e^{-\frac{k^2}{2}t}\frac{1}{h^2_{m,1}(Y_t)}\nabla h_{m,1}(Y_t) \cdot dB_t \Rightarrow \frac{1}{h_{m,1}(Y_\tau)}e^{-\frac{k^2}{2}\tau} = \frac{1}{h_{m,1}(x-\xi)} - \int_0^\tau e^{-\frac{k^2}{2}s}\frac{1}{h^2_{m,1}(Y_s)}\nabla h_{m,1}(Y_s) \cdot dB_s$$
$$\Rightarrow E^x\left(\frac{1}{h_{m,1}(Y_\tau)}e^{-\frac{k^2}{2}\tau}\right) = \frac{1}{j_m(k|x-\xi|)} \Rightarrow E^x\left(\frac{1}{j_m(k|Y_\tau|)P_m(\cos\Theta_\tau)}e^{-\frac{k^2}{2}\tau}\right) = \frac{1}{j_m(k|x-\xi|)}, \tag{25}$$

where the independence of Y_t, dB_t is again exploited. Let $\mathcal{W}_{\lambda'}$ denote the subset of the σ-algebra $\mathcal{F}$ representing the status of escaping from the lateral surface via points satisfying $|Y_\tau| < \lambda'|x-\xi|$. More clearly, we set

$$\mathcal{W}_{\lambda'} = \left\{\omega \in \Omega : \Theta_\tau(\omega) = \theta_{m,1} - \epsilon \text{ and } |Y_\tau(\omega)| < \lambda'|x-\xi|\right\}. \tag{26}$$

Then the set $\left[\{X_\tau \in \partial\tilde{D}^e_{m,\epsilon}(\xi)\}\right.$ and $\left.\{\Theta_\tau = \theta_{m,1} - \epsilon\}\right]$ appearing in the statement of the current proposition represents the subset of Ω supporting escaping from the lateral surface independently of the distance from the auxiliary point ξ; it is identified clearly with the set $\mathcal{W}_{\frac{e_m}{k|x-\xi|}}$, simply denoted by $\mathcal{W}$.

Similarly, it holds that $\left[\{X_\tau \in \partial\tilde{D}^e_{m,\epsilon}(\xi)\}\right.$ and $\{\Theta_\tau = \theta_{m,1} - \epsilon\}$ and $\left.\{|Y_\tau| < \lambda'|x-\xi|\}\right]$ $= \mathcal{W}_{\lambda'}$. The argument in expectation term of Equation (25) is positive and so by restriction over specific probability subsets, Expression (25) gives

$$\frac{1}{j_m(k\lambda'|x-\xi|)P_m(\cos(\theta_{m,1}-\epsilon))}E^x(e^{-\frac{k^2}{2}\tau}|\mathcal{W}_{\lambda'})P(\mathcal{W}_{\lambda'}) \leq \frac{1}{j_m(k|x-\xi|)}. \tag{27}$$

Applying Jensen's inequality for conditional expectations [14] to the convex function $e^{-\frac{k^2}{2}\tau}$, we find that

$$e^{-\frac{k^2}{2}E^x(\tau|\mathcal{W}_{\lambda'})}P(\mathcal{W}_{\lambda'}) \leq \frac{j_m(k\lambda'|x-\xi|)}{j_m(k|x-\xi|)}P_m(\cos(\theta_{m,1}-\epsilon)). \tag{28}$$

Given that $E^x(\tau|\mathcal{W}_{\lambda'}) = \frac{E^x(\tau\cap\{\mathcal{W}_{\lambda'}\})}{P(\mathcal{W}_{\lambda'})} \leq \frac{E^x(\tau)}{P(\mathcal{W}_{\lambda'})}$, Equation (28) becomes

$$\frac{P^x(\mathcal{W}_{\lambda'})}{e^{\frac{k^2E^x(\tau)}{2P(\mathcal{W}_{\lambda'})}}} \leq \frac{j_m(k\lambda'|x-\xi|)}{j_m(k|x-\xi|)}P_m(\cos(\theta_{m,1}-\epsilon)). \tag{29}$$

On the basis of Relation (18), the direct estimate $\frac{k^2}{2}E^x(\tau) \leq \frac{1}{2(2\delta+3)}\left(e_m^2 - k^2|x-\xi|^2\right) := \nu_m(k|x-\xi|)$ helps in modifying Equation (29) as follows

$$\Psi\left(\frac{P^x(\mathcal{W}_{\lambda'})}{\nu_m(k|x-\xi|)}\right) \leq \frac{1}{\nu_m(k|x-\xi|)}\frac{j_m(k\lambda'|x-\xi|)}{j_m(k|x-\xi|)}P_m(\cos(\theta_{m,1}-\epsilon)),$$

where $\Psi(x) = xe^{-\frac{1}{x}},\ x > 0$ is a well known increasing function with zero limiting value as $x \to 0$. Evoking the increasing inverse function $\Psi^{(-1)}$ (which also vanishes as its argument goes to zero), we find that

$$P^x(\mathcal{W}_{\lambda'}) \leq \nu_m(k|x-\xi|)\Psi^{(-1)}\left(\frac{1}{\nu_m(k|x-\xi|)}\frac{j_m(k\lambda'|x-\xi|)}{j_m(k|x-\xi|)}P_m(\cos(\theta_{m,1}-\epsilon))\right). \tag{30}$$

Clearly,

$$\begin{aligned} P^x(\mathcal{W}) &= P^x\left(\{X_\tau \in \partial\tilde{D}^e_{m,\epsilon}(\xi)\} \cap \{\Theta_\tau = \theta_{m,1}-\epsilon\}\right) \\ &\leq \nu_m(k|x-\xi|)\Psi^{(-1)}\left(\frac{1}{\nu_m(k|x-\xi|)}\frac{j_m(e_m)}{j_m(k|x-\xi|)}P_m(\cos(\theta_{m,1}-\epsilon))\right). \end{aligned} \tag{31}$$

Thanks to $\lim_{\epsilon\to 0} P_m(\cos(\theta_{m,1}-\epsilon)) = 0$ and the aforementioned properties of $\Psi^{(-1)}$, it holds that

$$\lim_{\epsilon\to 0} P^x\left(\{X_\tau \in \partial\tilde{D}^e_{m,\epsilon}(\xi)\} \cap \{\Theta_\tau = \theta_{m,1}-\epsilon\}\right) = 0. \tag{32}$$

□

The Estimates (30) and (31) are rigorous and ensure the convergence regime established in the above proposition but their intrinsic form is not directly exploitable when a rate of convergence is explored. To facilitate the analysis, we introduce a time threshold T and investigate its influence in cases where we consider the stochastic process with a life time less than T. In practice, the numerical experiments revealed that the driving term is strong enough to force a short finite time travel inside $\partial\tilde{D}^e_{m,\epsilon}(\xi)$. Paying attention to this situation we state and prove the next proposition.

Proposition 3. *If the domain of the stochastic process (15) is $\tilde{D}^e_{m,\epsilon}(\xi)$ and τ is the first exit time from this domain, then the probability of escaping from the lateral surface, instead of the cups, in finite time T has the estimate*

$$P^x\left(\{X_\tau \in \partial\tilde{D}^e_{m,\epsilon}(\xi)\} \cap \{\Theta_\tau = \theta_{m,1} - \epsilon\} \cap \{\tau < T\}\right) \leq e^{\frac{k^2}{2}T} \frac{j_m(e_m)}{j_m(k|x-\xi|)} P_m(\cos(\theta_{m,1} - \epsilon)). \tag{33}$$

In addition,

$$P^x\left(\{X_\tau \in \partial\tilde{D}^e_{m,\epsilon}(\xi)\} \cap \{|Y_\tau| < \lambda'|x-\xi|\} \cap \{\Theta_\tau = \theta_{m,1} - \epsilon\} \cap \{\tau < T\}\right) \leq e^{\frac{k^2}{2}T} \frac{j_m(k\lambda'|x-\xi|)}{j_m(k|x-\xi|)} P_m(\cos(\theta_{m,1} - \epsilon)).$$

Proof. Equation (25) gives that

$$\begin{aligned}
&E^x\left(\frac{1}{j_m(k|Y_\tau|)P_m(\cos\Theta_\tau)} e^{-\frac{k^2}{2}\tau} \,|\, \mathcal{W}_{\lambda'} \cap \{\tau < T\}\right) P^x(\mathcal{W}_{\lambda'} \cap \{\tau < T\}) \leq \frac{1}{j_m(k|x-\xi|)} \Rightarrow \\
&\frac{e^{-\frac{k^2}{2}T}}{j_m(k\lambda'|x-\xi|)P_m(\cos(\theta_{m,1} - \epsilon))} P^x(\mathcal{W}_{\lambda'} \cap \{\tau < T\}) \leq \frac{1}{j_m(k|x-\xi|)} \Rightarrow \\
&P^x(\mathcal{W}_{\lambda'} \cap \{\tau < T\}) \leq e^{\frac{k^2}{2}T} \frac{j_m(k\lambda'|x-\xi|)}{j_m(k|x-\xi|)} P_m(\cos(\theta_{m,1} - \epsilon)),
\end{aligned} \tag{34}$$

which coincides with the second result of the proposition. Equation (33) is a direct consequence of the result (34) if the selection $\lambda' = \frac{e_m}{k|x-\xi|}$ is adopted. □

The estimate (33) is useful only when the modification of the original cone is very small. Actually, the term $e^{\frac{k^2}{2}T} \frac{j_m(e_m)}{j_m(k|x-\xi|)}$ is always greater than unity and so only when ϵ is appropriately small does this probability estimate acquires a fruitful asymptotic content. Moreover, the result (34) merits its own attention since it assigns the appropriate probability to lateral escapes confined in the region $|Y_\tau| < \lambda'|x-\xi|$. In particular, when $\lambda' < 1$ the term $\frac{j_m(k\lambda'|x-\xi|)}{j_m(k|x-\xi|)}$ becomes significantly less than unity and contributes essentially to the determination of the probability estimate, verifying the small likelihood of trajectories orientated inwards concerning the vertex of the cone.

The next issue is to estimate the probabilities of escaping from the possible exit surfaces in the case of the domain $\tilde{D}^{e,\gamma}_m(\xi) = D^e \cap \mathcal{K}_{m+\gamma} \cap \{z \in \mathbb{R}^n : \eta < |z-\xi| < L\}$. In fact, it is now possible to give strict values to the probabilities of hitting the spherical cups of the structure $\tilde{D}^{e,\gamma}_m(\xi)$.

Proposition 4. *Let the height of $\tilde{D}^{e,\gamma}_m(\xi)$ be selected as $L = \frac{e_m}{k}$ and select a small variable $0 < a << 1$. Furthermore, let the surface of the inner spherical cup S_η belong to D^e. Referring to the stochastic process Y_t generated from a point x of the axis of the cone and evolving in $\tilde{D}^{e,\gamma}_m(\xi)$, it holds that*

$$P^x\left[|Y_\tau| = \frac{e_m}{k}\right] \geq \frac{j_m(e_m)}{j_m(k|x-\xi|)} \frac{[j_{m+\gamma}(k|x-\xi|)y_{m+\gamma}(k\eta) - j_{m+\gamma}(k\eta)y_{m+\gamma}(k|x-\xi|)]}{[j_{m+\gamma}(e_m)y_{m+\gamma}(k\eta) - j_{m+\gamma}(k\eta)y_{m+\gamma}(e_m)]} \tag{35}$$

$$P^x[\{|Y_\tau| = \eta\} \cap \{\Theta_\tau < \vartheta_{m+\gamma}(a)\}] \leq \frac{1}{(1-a)} \frac{j_m(k\eta)}{j_m(k|x-\xi|)} \frac{j_{m+\gamma}(e_m)|y_{m+\gamma}(k|x-\xi|)|}{[j_{m+\gamma}(e_m)|y_{m+\gamma}(k\eta)| - j_{m+\gamma}(k\eta)|y_{m+\gamma}(e_m)|]}, \tag{36}$$

where the angle $\vartheta_{m+\gamma}(a)$ is slightly smaller than the angle $\theta_{m+\gamma,1}$ defining the lateral surface of $\tilde{D}^{e,\gamma}_m(\xi)$.

Proof. We consider the auxiliary function $v(y) = j_{m+\gamma}(k|y|)P_{m+\gamma}(\cos(\theta))$, where again we use the spherical coordinates of the local coordinate system attached to the cone $\mathcal{K}_m$.

Clearly, v belongs to $\ker(\Delta + k^2)$ inside $\tilde{D}_m^{e,\gamma}(\xi)$ and vanishes on the lateral surface of region $\tilde{D}_m^{e,\gamma}(\xi)$. We apply once again Dynkin's formula for the field $\frac{v}{h_{m,1}}$, obtaining

$$E^x\left[\frac{v(Y_\tau)}{h_{m,1}(Y_\tau)}\right] = \frac{v(x-\xi)}{h_{m,1}(x-\xi)} + E^x\left[\int_0^\tau A\left(\frac{v(Y_\tau)}{h_{m,1}(Y_s)}\right)ds\right]. \tag{37}$$

Denoting $h = h_{m,1}$, we find that

$$A\left(\frac{v}{h}\right) = \frac{\nabla h}{h}\cdot\nabla\left(\frac{v}{h}\right) + \frac{1}{2}\Delta\left(\frac{v}{h}\right) = \frac{h\Delta(\frac{v}{h}) + 2\nabla h\cdot\nabla(\frac{v}{h}) + (\frac{v}{h})\Delta h - (\frac{v}{h})\Delta h}{2h} = \frac{\Delta v + k^2 v}{2h} = 0.$$

So Equation (37) becomes

$$\frac{j_{m+\gamma}(k|x-\xi|)}{j_m(k|x-\xi|)} = E^x\left[\frac{v(Y_\tau)}{h_{m,1}(Y_\tau)}\right]. \tag{38}$$

Exploiting that $P_{m+\gamma}$ vanishes on the lateral surface, we split the equation above as follows

$$\frac{j_{m+\gamma}(k|x-\xi|)}{j_m(k|x-\xi|)} = \frac{j_{m+\gamma}(kL)}{j_m(kL)}E^x_{\text{ext}}\left[\frac{P_{m+\gamma}(\cos(\Theta_\tau))}{P_m(\cos(\Theta_\tau))}\right] + \frac{j_{m+\gamma}(k\eta)}{j_m(k\eta)}E^x_{\text{int}}\left[\frac{P_{m+\gamma}(\cos(\Theta_\tau))}{P_m(\cos(\Theta_\tau))}\right] \tag{39}$$

where the subscripts in expectations denote the two cups of the region $\tilde{D}_m^e(\xi)$. Working similarly with the auxiliary field $\tilde{v}(y) = y_{m+\gamma}(k|y|)P_{m+\gamma}(\cos(\theta))$ (instead of v), we infer that

$$\frac{y_{m+\gamma}(k|x-\xi|)}{j_m(k|x-\xi|)} = \frac{y_{m+\gamma}(kL)}{j_m(kL)}E^x_{\text{ext}}\left[\frac{P_{m+\gamma}(\cos(\Theta_\tau))}{P_m(\cos(\Theta_\tau))}\right] + \frac{y_{m+\gamma}(k\eta)}{j_m(k\eta)}E^x_{\text{int}}\left[\frac{P_{m+\gamma}(\cos(\Theta_\tau))}{P_m(\cos(\Theta_\tau))}\right]. \tag{40}$$

So far we have selected the height of the cone L equal to $\frac{e_m}{k}$. In fact, the parameter e_m defines a range of radial distance, inside which the crucial part of the driving term $\mathcal{H}_m$ remains strictly positive. In addition, inside the interval $(0, e_m)$, the spherical Legendre functions j_m, y_m are permanently opposite and free of zeros. Actually the same situation holds for the pair $j_{m+\gamma}, y_{m+\gamma}$ of the Bessel functions of order $m+\gamma$ since as mentioned above the sequence e_m increases. Substituting then again $L = \frac{e_m}{k}$ and solving the algebraic Systems (39) and (40), we find the unique solution

$$E^x_{\text{ext}}\left[\frac{P_{m+\gamma}(\cos(\Theta_\tau))}{P_m(\cos(\Theta_\tau))}\right] = \mathcal{A}_m(x,\xi,\eta) := \frac{j_m(e_m)}{j_m(k|x-\xi|)}\frac{[j_{m+\gamma}(k|x-\xi|)y_{m+\gamma}(k\eta) - j_{m+\gamma}(k\eta)y_{m+\gamma}(k|x-\xi|)]}{[j_{m+\gamma}(e_m)y_{m+\gamma}(k\eta) - j_{m+\gamma}(k\eta)y_{m+\gamma}(e_m)]}, \tag{41}$$

$$E^x_{\text{int}}\left[\frac{P_{m+\gamma}(\cos(\Theta_\tau))}{P_m(\cos(\Theta_\tau))}\right] = \mathcal{B}_m(x,\xi,\eta) := \frac{j_m(k\eta)}{j_m(k|x-\xi|)}\frac{[j_{m+\gamma}(e_m)y_{m+\gamma}(k|x-\xi|) - j_{m+\gamma}(k|x-\xi|)y_{m+\gamma}(e_m)]}{[j_{m+\gamma}(e_m)y_{m+\gamma}(k\eta) - j_{m+\gamma}(k\eta)y_{m+\gamma}(e_m)]}. \tag{42}$$

The denominator $\mathcal{D} := j_{m+\gamma}(e_m)y_{m+\gamma}(k\eta) - j_{m+\gamma}(k\eta)y_{m+\gamma}(e_m)$ in these expressions cannot be zero due to the monotonicity properties of the involved functions. In most cases $\mathcal{D} \approx j_{m+\gamma}(e_m)y_{m+\gamma}(k\eta)$.

We notice that the function $\frac{P_{m+\gamma}(\chi)}{P_m(\chi)}$ increases in $[\chi_{m+\gamma,1}, 1]$, taking values from 0 to 1. More precisely, it rapidly increases in the vicinity of $\chi_{m+\gamma,1}$ and then approaches unity almost horizontally. These qualitative results concerning the monotonicity of $\frac{P_{m+\gamma}(\chi)}{P_m(\chi)}$ guarantee that there always exists a threshold $\zeta_{m+\gamma} = \cos(\vartheta_{m+\gamma})$ greater but very close (the angle $\vartheta_{m+\gamma}$ is slightly less than $\theta_{m+\gamma,1}$) to $\chi_{m+\gamma,1}$, such that $\frac{P_{m+\gamma}(\chi)}{P_m(\chi)} > 1-a$ when $\chi \in [\vartheta_{m+\gamma}, 1]$ and $0 < a << 1$. These remarks help first in exploiting Equation (42) as follows

$$(1-a)E^x_{int}[\{\Theta_\tau < \vartheta_{m+\gamma}(a)\}] \le \frac{j_m(k\eta)}{j_m(k|x-\xi|)}\frac{[j_{m+\gamma}(e_m)y_{m+\gamma}(k|x-\xi|) - j_{m+\gamma}(k|x-\xi|)y_{m+\gamma}(e_m)]}{[j_{m+\gamma}(e_m)y_{m+\gamma}(k\eta) - j_{m+\gamma}(k\eta)y_{m+\gamma}(e_m)]} \Rightarrow$$

$$P^x[\{|Y_\tau| = \eta\}\cap\{\Theta_\tau < \vartheta_{m+\gamma}(a)\}] \le \frac{1}{(1-a)}\frac{j_m(k\eta)}{j_m(k|x-\xi|)}\frac{j_{m+\gamma}(e_m)|y_{m+\gamma}(k|x-\xi|)|}{[j_{m+\gamma}(e_m)|y_{m+\gamma}(k\eta)| - j_{m+\gamma}(k\eta)|y_{m+\gamma}(e_m)|]}, \tag{43}$$

coinciding with Equation (36). On the other hand, Equation (41) provides easily

$$E^x_{\text{ext}}[1] \geq \mathcal{A}_m(x,\xi,\eta) \Rightarrow$$
$$P^x\left[|Y_\tau| = \frac{e_m}{k}\right] \geq \frac{j_m(e_m)}{j_m(k|x-\xi|)} \frac{[j_{m+\gamma}(k|x-\xi|)y_{m+\gamma}(k\eta) - j_{m+\gamma}(k\eta)y_{m+\gamma}(k|x-\xi|)]}{[j_{m+\gamma}(e_m)y_{m+\gamma}(k\eta) - j_{m+\gamma}(k\eta)y_{m+\gamma}(e_m)]},$$

as stated in Equation (35). □

Remark 1. *It is worthwhile to notice that Equation (43) predicts, in most cases, negligible values for the probability of hitting on the interior spherical small cup. Indeed, having in mind that* $k\eta < k|x-\xi| < e_m$ *and thus adopting the reasonable simplification* $j_{m+\gamma}(e_m)|y_{m+\gamma}(k\eta)| - j_{m+\gamma}(k\eta)|y_{m+\gamma}(e_m)| \approx j_{m+\gamma}(e_m)|y_{m+\gamma}(k\eta)|$*, we obtain that*

$$P^x[\{|Y_\tau| = \eta\} \cap \{\Theta_\tau < \vartheta_{m+\gamma}(a)\}] \leq \frac{1}{1-a} \frac{j_m(k\eta)}{j_m(k|x-\xi|)} \frac{|y_{m+\gamma}(k|x-\xi|)|}{|y_{m+\gamma}(k\eta)|}.$$

In the case that the arguments $k\eta$ *and* $k|x-\xi|$ *belong to the realm of validity of asymptotic formulae for the involved special functions, we find that*

$$P^x[\{|Y_\tau| = \eta\} \cap \{\Theta_\tau < \vartheta_{m+\gamma}(a)\}] \leq \frac{1}{1-a}\left(\frac{\eta}{|x-\xi|}\right)^{2m+\gamma+1},$$

which avoids being negligible only when the starting point is forced to be located closely above the inner cup. The situation remains unaltered even if the arguments $k\eta$ *and* $k|x-\xi|$ *escape the asymptotic realm as the investigation of special functions imposes.*

Furthermore, Equation (35) can be easily weakened to offer a simpler (though underestimated) lower bound:

$$P^x\left[|Y_\tau| = \frac{e_m}{k}\right] \geq \frac{j_m(e_m)}{j_m(k|x-\xi|)} \frac{j_{m+\gamma}(k|x-\xi|)}{j_{m+\gamma}(e_m)}\left[1 - \frac{j_{m+\gamma}(k\eta)}{j_{m+\gamma}(k|x-\xi|)} \frac{y_{m+\gamma}(k|x-\xi|)}{y_{m+\gamma}(k\eta)}\right]. \quad (44)$$

When the point x *is even slightly detached from the inner cup it holds that* $\frac{j_{m+\gamma}(k\eta)}{j_{m+\gamma}(k|x-\xi|)} \frac{y_{m+\gamma}(k|x-\xi|)}{y_{m+\gamma}(k\eta)}$ $<< 1$*. Then the lower bound of the probability* P^x_{ext} *obtains the form* $\frac{j_m(e_m)}{j_m(k|x-\xi|)} \frac{j_{m+\gamma}(k|x-\xi|)}{j_{m+\gamma}(e_m)}$*. It is remarkable that this ratio involves the starting point and the height of the exterior cup alone. It is obvious that* $\lim_{\gamma\to 0} \frac{j_m(e_m)}{j_m(k|x-\xi|)} \frac{j_{m+\gamma}(k|x-\xi|)}{j_{m+\gamma}(e_m)} = 1$*, a fact assuring the total accumulation of hitting points on the exterior cup when* γ *converges to zero.*

For completeness reasons, we state the following result.

Proposition 5. *Let the assumptions of Proposition 4 be valid except that the initial point* x *of the process is not located necessarily on the z-axis but potentially forms a polar angle* θ_0 *with it. Then the probability of escaping from the lateral surface obeys the rule*

$$P^x\left[\Theta_\tau = \theta_{m+\gamma,1}\right] \leq 1 - \frac{P_{m+\gamma}(\cos(\theta_0))}{P_m(\cos(\theta_0))}(\mathcal{A}_m(x,\xi,\eta) + \mathcal{B}_m(x,\xi,\eta)). \quad (45)$$

Proof. Imitating the arguments presented in Proposition 4, we easily see that the detaching of x from the cone axis has the consequence of changing Formula (38) as follows:

$$\frac{j_{m+\gamma}(k|x-\xi|)}{j_m(k|x-\xi|)} \frac{P_{m+\gamma}(\cos(\theta_0))}{P_m(\cos(\theta_0))} = E^x\left[\frac{v(Y_\tau)}{h_{m,1}(Y_\tau)}\right] \quad (46)$$

Proceeding similarly, we find that Equations (41) and (42) are replaced by relations

$$E^x_{\text{ext}}\left[\frac{P_{m+\gamma}(\cos(\Theta_\tau))}{P_m(\cos(\Theta_\tau))}\right] = \frac{P_{m+\gamma}(\cos(\theta_0))}{P_m(\cos(\theta_0))}\mathcal{A}_m(x,\xi,\eta)$$
$$E^x_{\text{int}}\left[\frac{P_{m+\gamma}(\cos(\Theta_\tau))}{P_m(\cos(\Theta_\tau))}\right] = \frac{P_{m+1}(\cos(\theta_0))}{P_m(\cos(\theta_0))}\mathcal{B}_m(x,\xi,\eta),$$

from which we deduce that

$$P^x\left[|Y_\tau| = \frac{e_m}{k}\right] \geq \frac{P_{m+\gamma}(\cos(\theta_0))}{P_m(\cos(\theta_0))}\mathcal{A}_m(x,\xi,\eta) \text{ and } P^x[|Y_\tau| = \eta] \geq \frac{P_{m+\gamma}(\cos(\theta_0))}{P_m(\cos(\theta_0))}\mathcal{B}_m(x,\xi,\eta).$$

Consequently

$$P^x[\Theta_\tau = \theta_{m+\gamma,1}] = 1 - P^x\left[|Y_\tau| = \frac{e_m}{k}\right] - P^x[|Y_\tau| = \eta] \leq 1 - \frac{P_{m+\gamma}(\cos(\theta_0))}{P_m(\cos(\theta_0))}(\mathcal{A}_m(x,\xi,\eta) + \mathcal{B}_m(x,\xi,\eta)).$$

□

The closer the angle θ_0 is laid to the zero value, the more $P^x[\Theta_\tau = \theta_{m+\gamma,1}]$ is suppressed to zero, under the validity of the relation $\mathcal{A}_m(x,\xi,\eta) + \mathcal{B}_m(x,\xi,\eta) \approx 1$, induced by Remark 1. In contrast to that, when θ_0 approaches $\theta_{m+\gamma,1}$, the factor $\frac{P_{m+\gamma}(\cos(\theta_0))}{P_m(\cos(\theta_0))}$ goes to zero, taking down with it the probabilities $P^x\left[|Y_\tau| = \frac{e_m}{k}\right]$ and $P^x[|Y_\tau| = \eta]$ and amplifying drastically the appearance of lateral crossings. This is the reason we insist on locating the starting point of the stochastic process on the cone axis and then eventually eliminate the probability of lateral surface hitting.

So far, we have studied some basic qualitative properties of the trajectories representing the solutions of the underlying stochastic differential equations and derived estimations for some crucial probabilities concerning the hitting points of these trajectories on the components of the boundaries. Two cases have preoccupied our interest: The general case $\tilde{D}^e_{m,\epsilon}(\xi)$ as well as the more special conical region $\tilde{D}^{e,\gamma}_m(\xi)$. It will be clear during the implementation of the method that a result of the type (31) pertaining to the first case would be useful—actually in a stronger form—even for the second case as well. In this direction, we state and prove the following lemmata.

Lemma 1. *It holds that*

$$\ln\left(\frac{h_{m,1}(Y_\tau)}{j_m(k|x-\xi|)}\right) = \frac{1}{2}\int_0^\tau \frac{|\nabla h_{m,1}(Y_t)|^2}{h^2_{m,1}(Y_t)}dt - \frac{k^2}{2}\tau + \int_0^\tau \frac{\nabla h_{m,1}(Y_t)}{h_{m,1}(Y_t)} \cdot dB_t \tag{47}$$

Proof. The Itô formula gives

$$d(\ln h_{m,1}(Y_t)) = \frac{\nabla h_{m,1}(Y_t)}{h_{m,1}(Y_t)} \cdot dY_t + \frac{1}{2}\left(\frac{\nabla\nabla h_{m,1}(Y_t)}{h_{m,1}(Y_t)} - \frac{\nabla h_{m,1}(Y_t)\nabla h_{m,1}(Y_t)}{h^2_{m,1}(Y_t)}\right) : dY_t dY_t =$$
$$\frac{1}{2}\frac{|\nabla h_{m,1}(Y_t)|^2}{h^2_{m,1}(Y_t)}dt + \frac{1}{2}\frac{\Delta h_{m,1}(Y_t)}{h_{m,1}(Y_t)}dt + \frac{\nabla h_{m,1}(Y_t)}{h_{m,1}(Y_t)} \cdot dB_t = \frac{1}{2}\frac{|\nabla h_{m,1}(Y_t)|^2}{h^2_{m,1}(Y_t)}dt - \frac{k^2}{2}dt + \frac{\nabla h_{m,1}(Y_t)}{h_{m,1}(Y_t)} \cdot dB_t,$$

from where we obtain the sought result via time integration. □

Lemma 2. *For every $\zeta \in \mathbb{R}$, it holds that*

$$E^x\left(\frac{1}{h^{\zeta^2}_{m,1}(Y_\tau)}e^{\left[\frac{\zeta(\zeta-1)}{2}\int_0^\tau \frac{\nabla h_{m,1}(Y_t)}{h_{m,1}(Y_t)} \cdot dB_t - \frac{k^2\zeta^2}{2}\tau\right]}\right) = \frac{1}{j^{\zeta^2}_m(k|x-\xi|)} \tag{48}$$

Proof. Equation (24) is equivalent to

$$d\left(\frac{1}{h_{m,1}^{\zeta}(Y_t)}e^{-\frac{\zeta}{2}\int_0^t\left[k^2+(\zeta-1)\frac{|\nabla h_{m,1}(Y_s)|^2}{h_{m,1}^2(Y_s)}\right]ds}\right)=-\frac{\zeta}{h_{m,1}^{\zeta+1}}\nabla h_{m,1}\cdot dB_t\, e^{-\frac{\zeta}{2}\int_0^t\left[k^2+(\zeta-1)\frac{|\nabla h_{m,1}(Y_s)|^2}{h_{m,1}^2(Y_s)}\right]ds}$$

Integrating over time until the first exit time and taking the expectation value as usual, we obtain

$$E^x\left(\frac{1}{h_{m,1}^{\zeta}(Y_\tau)}e^{-\frac{\zeta}{2}\int_0^\tau\left[k^2+(\zeta-1)\frac{|\nabla h_{m,1}(Y_t)|^2}{h_{m,1}^2(Y_t)}\right]dt}\right)=\frac{1}{j_m^{\zeta}(k|x-\xi|)} \tag{49}$$

The argument inside the expectation of the last expression can be handled via the previous lemma as follows

$$\frac{1}{h_{m,1}^{\zeta}(Y_\tau)}e^{-\frac{\zeta}{2}\int_0^\tau\left[k^2+(\zeta-1)\frac{|\nabla h_{m,1}(Y_t)|^2}{h_{m,1}^2(Y_t)}\right]dt}=\frac{j_{m,1}^{\zeta(\zeta-1)}(k|x-\xi|)}{h_{m,1}^{\zeta^2}(Y_\tau)}e^{\frac{\zeta(\zeta-1)}{2}\int_0^\tau\frac{\nabla h_{m,1}(Y_t)}{h_{m,1}(Y_t)}\cdot dB_t-\frac{k^2\zeta^2}{2}\tau} \tag{50}$$

Combining Equations (49) and (50), we find that

$$E^x\left(\frac{1}{h_{m,1}^{\zeta^2}(Y_\tau)}e^{\left[\frac{\zeta(\zeta-1)}{2}\int_0^\tau\frac{\nabla h_{m,1}(Y_t)}{h_{m,1}(Y_t)}\cdot dB_t-\frac{k^2\zeta^2}{2}\tau\right]}\right)=\frac{1}{j_m^{\zeta^2}(k|x-\xi|)}.$$

□

The next proposition extends the main result of Proposition 3 not only for referring to the alternative conical structure but mainly for ameliorating the rate of convergence as γ diminishes:

Proposition 6. *If the domain of the stochastic process (15) is $\tilde{D}_m^{e,\gamma}(\xi)$ and τ is the first exit time from this domain, then the probability of escaping from the lateral surface, instead of the cups, in finite time T has the estimate*

$$P^x\left(\{X_\tau\in\partial\tilde{D}_m^{e,\gamma}(\xi)\}\cap\{\Theta_\tau=\theta_{m+\gamma,1}\}\cap\{\tau<T\}\right)\le e^{\frac{k^2\zeta}{2}T}\left(\frac{j_m(e_m)}{j_m(k|x-\xi|)}\right)^{\zeta}P_m^{\zeta}(\cos(\theta_{m+\gamma,1})), \tag{51}$$

for any real $\zeta>1$.

Proof. We consider the set

$$\mathcal{V}_T=\{\omega\in\Omega:\{X_\tau(\omega)\in\partial\tilde{D}_m^{e,\gamma}(\xi)\}\cap\{\Theta_\tau(\omega)=\theta_{m+\gamma,1}\}\cap\{\tau(\omega)<T\}\}.$$

Thanks to the monotonicity of the spherical Bessel function, Jensen's inequality for conditional expectations and the independence of Y_t, dB_t, Equation (48) is transformed as follows

$$\frac{e^{-\frac{k^2\zeta^2}{2}T}}{j_m^{\zeta^2}(e_m)P_m^{\zeta^2}(\cos(\theta_{m+\gamma,1}))}E^x\left(e^{\left[\frac{\zeta(\zeta-1)}{2}\int_0^\tau\frac{\nabla h_{m,1}(Y_t)}{h_{m,1}(Y_t)}\cdot dB_t\right]}|\mathcal{V}_T\right)P^x(\mathcal{V}_T)\le\frac{1}{j_m^{\zeta^2}(k|x-\xi|)}\Rightarrow$$

$$e^{-\frac{k^2\zeta^2}{2}T}e^{\frac{\zeta(\zeta-1)}{2}E^x\left[\int_0^\tau\frac{\nabla h_{m,1}(Y_t)}{h_{m,1}(Y_t)}\cdot dB_t|\mathcal{V}_T\right]}P^x(\mathcal{V}_T)\le\frac{j_m^{\zeta^2}(e_m)}{j_m^{\zeta^2}(k|x-\xi|)}P_m^{\zeta^2}(\cos(\theta_{m+\gamma,1}))\Rightarrow$$

$$P^x(\mathcal{V}_T)\le e^{\frac{k^2\zeta^2}{2}T}\frac{j_m^{\zeta^2}(e_m)}{j_m^{\zeta^2}(k|x-\xi|)}P_m^{\zeta^2}(\cos(\theta_{m+\gamma,1})) \tag{52}$$

Renaming ζ^2 to ζ we have what the proposition states. $\square$

We mention here that we restrict ourselves to the interesting case $\zeta > 1$. Actually, the result with $\zeta < 1$ is an immediate consequence of Proposition 3 with $\epsilon = \theta_{m,1} - \theta_{m+\gamma,1}$ sufficiently small so that the right hand side of Equation (33) is less than unity. The selection of ζ is related with the total travel time T. The exponential term remains small when the term $2\pi^2\zeta \frac{T}{\lambda^2}$ does, where the wave-length λ of the process appears. The quantity $\frac{T}{\lambda^2}$ commonly emerges in stochastic processes involving appropriately the space and time dimensions.

3.2. On Deriving Stochastic Representations for the Scattered Field

At this point, the involvement of the physical field representing the scattered wave u presented in Section 2 takes place. We recall that this field belongs to the kernel of the Helmholtz operator. Our aim is to embed appropriately this field in Dynkin's calculus, which has already profited throughout the treatment of the stochastic process under consideration. More precisely, considering the field $w(x) = \frac{u(x)}{h_{m,1}(x-\xi)}$, $j = 1, 2$, we are in a position to apply once more Dynkin's formula leading to the stochastic representation

$$E^x\left[\frac{u(X_\tau)}{h_{m,1}(Y_\tau)}\right] = \frac{u(x)}{h_{m,1}(x-\xi)} + E^x\left[\int_0^\tau A\left(\frac{u(X_s)}{h_{m,1}(Y_s)}\right)ds\right],\ j = 1,2. \tag{53}$$

Denoting $h = h_{m,1}$, we find that

$$A\left(\frac{u}{h}\right) = \frac{\nabla h}{h}\cdot\nabla\left(\frac{u}{h}\right) + \frac{1}{2}\Delta\left(\frac{u}{h}\right) = \frac{h\Delta\left(\frac{u}{h}\right) + 2\nabla h\cdot\nabla\left(\frac{u}{h}\right) + \left(\frac{u}{h}\right)\Delta h - \left(\frac{u}{h}\right)\Delta h}{2h} = \frac{\Delta u + k^2 u}{2h} = 0.$$

So Equation (53) becomes

$$\frac{u(x)}{j_m(k|x-\xi|)} = E^x\left[\frac{u(X_\tau)}{h_{m,1}(Y_\tau)}\right] \Rightarrow u(x) = j_m(k|x-\xi|)E^x\left[\frac{u(X_\tau)}{h_{m,1}(Y_\tau)}\right]. \tag{54}$$

Working in $\tilde{D}_m^{e,\gamma}(\xi)$, the last relation obtains the form

$$\begin{aligned} u(x) \quad &= \quad \frac{j_m(k|x-\xi|)}{j_m(e_m)}E^x_{\text{ext}}\left[\frac{u(X_\tau)}{P_m(\cos(\Theta_\tau))}\right] + \frac{j_m(k|x-\xi|)}{j_m(k\eta)}E^x_{\text{int}}\left[\frac{u(X_\tau)}{P_m(\cos(\Theta_\tau))}\right] \\ &+ \quad \frac{j_m(k|x-\xi|)}{P_m(\cos(\theta_{m+\gamma,1}))}E^x_{\text{lat}}\left[\frac{u(X_\tau)}{j_m(k|Y_\tau|)}\right],\ x \in \tilde{D}_m^{e,\gamma}(\xi) \end{aligned} \tag{55}$$

where we have taken into account the less probable but still possible event of stochastic escaping via the lateral surface of $\tilde{D}_m^{e,\gamma}(\xi)$.

The Representation (55) constitutes one of the fundamental results of this work and will be a subject of investigation during the examination of the inverse scattering problem. It has a local character since it is valid in a conical region $\tilde{D}_m^{e,\gamma}(\xi)$ surrounding point x and defines a specific portion of the exterior space. It constitutes a stochastic representation of the value of physical field in the point x, involving three terms corresponding to stochastically first time escaping events from the two spherical cups and the lateral surface of the cone. The severe or mild implication of every portion of the manifolds, where escaping takes place, has been revealed previously in this section. In brief terms, the Representation (55) favors the information offered in the exterior cup at the same time that it suppresses the importance of information that has taken place on the inner cup and eventually eliminates the involvement of the lateral surface. So this representation seems to be more adequate when we are interested in deriving a continuation of the remote field to the near field.

The immediate question arising on the basis of this discussion is whether there exists another stochastic representation giving priority to information on the interior cup and suppressing the involvement of data on the exterior spherical shell. This representation would have the character of a near to remote field transformation. This is actually accomplished by giving a primitive role to the auxiliary function $h_{m,2}(Y_t) = P_m(\hat{n} \cdot Y_t/|Y_t|)\mathcal{Q}_{m,2}(k|Y_t|) = P_m(\cos(\Theta_t))y_m(k|Y_t|)$ instead of $h_{m,1}(Y_t)$, which has been exploited so far. Taking advantage of the recurrence relation of spherical Bessel functions, we can transform Equation (13) in the following form

$$d\widetilde{Y}_t = \widetilde{\mathcal{H}}_m(k|Y_t|)\frac{\widetilde{Y}_t}{|\widetilde{Y}_t|^2}dt - \frac{\sin(\widetilde{\Theta}_t)P'_m(\cos(\widetilde{\Theta}_t))}{|\widetilde{Y}_t|P_m(\cos(\widetilde{\Theta}_t))}\hat{\widetilde{\Theta}}_t dt + dB_t, \tag{56}$$

with

$$\widetilde{\mathcal{H}}_m(\lambda) := \frac{\lambda y_{m-1}(\lambda)}{y_m(\lambda)} - (m+1), \ \ \lambda > 0. \tag{57}$$

This radial driving term is now negative (Figure 3) and has opposite behavior compared to $\mathcal{H}_m$. It is not the goal of this work to repeat all the theoretical investigation for this new stochastic differential System (56) but it is now recognizable to follow the main characteristics of the stochastic trajectories ruled by the negative driving term (57).

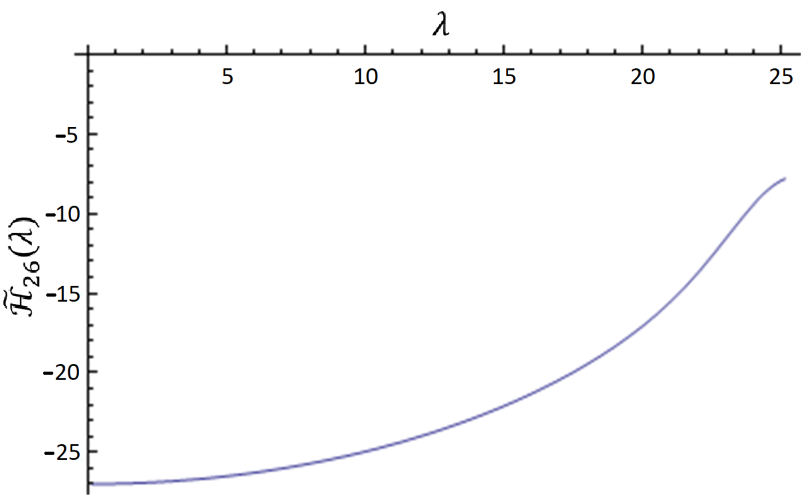

Figure 3. The increasing negative function $\widetilde{\mathcal{H}}_m(\lambda)$ for $m = 26$.

We remark easily, imitating the arguments presented in Proposition 1, that $E^x(|Y_\tau|^2) < |x - \xi|^2$ and so we expect an inward directivity of the new set of trajectories. Actually, in the new situation, the point ξ is not a repellent point but an attractor for the stochastic paths. Indeed, a straightforward application once again of the concepts presented in Proposition 4 leads to the estimations

$$P^x\left[\left\{|Y_\tau| = \frac{e_m}{k}\right\} \cap \{\Theta_\tau < \theta_{m+\gamma}(a)\}\right] \leq \frac{1}{(1-a)}\widetilde{\mathcal{A}}_m(x,\xi,\eta) \text{ and } P^x[\{|Y_\tau| = \eta\}] \geq \widetilde{\mathcal{B}}_m(x,\xi,\eta) \tag{58}$$

with

$$\widetilde{\mathcal{A}}_m(x,\xi,\eta) = \frac{y_m(e_m)}{y_m(k|x-\xi|)}\frac{[j_{m+\gamma}(k|x-\xi|)y_{m+\gamma}(k\eta) - j_{m+\gamma}(k\eta)y_{m+\gamma}(k|x-\xi|)]}{[j_{m+\gamma}(e_m)y_{m+\gamma}(k\eta) - j_{m+\gamma}(k\eta)y_{m+\gamma}(e_m)]}$$

$$\widetilde{\mathcal{B}}_m(x,\xi,\eta) = \frac{y_m(k\eta)}{y_m(k|x-\xi|)}\frac{[j_{m+\gamma}(e_m)y_{m+\gamma}(k|x-\xi|) - j_{m+\gamma}(k|x-\xi|)y_{m+\gamma}(e_m)]}{[j_{m+\gamma}(e_m)y_{m+\gamma}(k\eta) - j_{m+\gamma}(k\eta)y_{m+\gamma}(e_m)]}.$$

As special function properties reveal, $\widetilde{\mathcal{B}}_m(x,\xi,\eta)$ is, for most of the parameter cases, close to unity, while $\widetilde{\mathcal{A}}_m(x,\xi,\eta)$ lies in the vicinity of zero. Actually, we meet here the mirror situation, in which the trajectories starting from the axial point x converge inwards, attracted by the vertex ξ.

Working in $\tilde{D}_m^{e,\gamma}(\xi)$, we are in a position to present, in a way analogous with Equation (55), the representation of the scattered field in terms of the inward directed stochastic process:

$$\begin{aligned} u(x) &= \frac{y_m(k|x-\xi|)}{y_m(e_m)} E_{\text{ext}}^x \left[\frac{u(\widetilde{X}_\tau)}{P_m(\cos(\widetilde{\Theta}_\tau))} \right] + \frac{y_m(k|x-\xi|)}{y_m(k\eta)} E_{\text{int}}^x \left[\frac{u(\widetilde{X}_\tau)}{P_m(\cos(\widetilde{\Theta}_\tau))} \right] \\ &+ \frac{y_m(k|x-\xi|)}{P_m(\cos(\theta_{m+\gamma,1}))} E_{\text{lat}}^x \left[\frac{u(\widetilde{X}_\tau)}{y_m(k|\widetilde{Y}_\tau|)} \right], \; x \in \tilde{D}_m^{e,\gamma}(\xi) \end{aligned} \tag{59}$$

The fundamental Expressions (55) and (59) give the essential basis to design the geometric characteristics of the conical structure. A common feature in these expressions is the presence of the ratios of spherical Bessel functions defined on the point x as well as on the external and internal surface of the cone. These fractions can obtain very unbalanced values in the case that the position arguments are chosen arbitrarily. This is expected since these coefficients multiply expectation values of different orders due to the imposed conditional stochastic laws. So the selection of the geometrical characteristics of the detached conical region should obey the necessity to allow high sensitivity on revealing all types of data. In addition, the third terms in both representations incorporate a ratio between two controversial terms: The expectation value over the very few lateral escaping points and the very small value of the Legendre term $P_m(\cos(\theta_{m+\gamma,1}))$. This is a very interesting tag of war, whose investigation has caused the probabilistic analysis leading to Proposition 6. Actually, apart from the possibly large period of time T, the mentioned ratio is proportional to $P_m^{\zeta-1}(\cos(\theta_{m+\gamma,1}))$, $\zeta > 1$, which converges to 0 as $\gamma \to 0$. These and relevant matters merit special treatment when application of the method takes place in the next section.

The Representations (55) and (59) have been built on the basis of, respectively, strongly outward and inward moving stochastic trajectories. They develop by nature a strong preference to represent the field at x by data confined in the far field domain or the near field region, respectively. What remains is to explore the possibility of constructing a representation giving an equivalent role to the spherical cups and still deteriorating the role of the lateral surface. This can be realized via the implication of a modified driving term that stemmed from a linear combination of the spherical Bessel functions j_m and y_m. In fact, we start with the modified auxiliary function $g_m(\lambda) = C_m j_m(\lambda) - y_m(\lambda)$, where the mixture coefficient will be determined methodologically later on. This radial function gives birth to the Helmholtz equation solution $h_{m,3}(\check{Y}_t) = g_m(k|\check{Y}_t|) P_m(\cos \check{\Theta}_t)$, which as usual generates the set of stochastic differential equations

$$d\check{Y}_t = \check{\mathcal{H}}_m(k|\check{Y}_t|) \frac{\check{Y}_t}{|\check{Y}_t|^2} dt - \frac{\sin(\check{\Theta}_t) P_m'(\cos(\check{\Theta}_t))}{|\check{Y}_t| P_m(\cos(\check{\Theta}_t))} \widehat{\check{\Theta}}_t dt + dB_t, \tag{60}$$

where

$$\check{\mathcal{H}}_m(\lambda) := \frac{\lambda g_m'(\lambda)}{g_m(\lambda)} = \frac{\lambda [C_m j_{m-1}(\lambda) - y_{m-1}(\lambda)]}{g_m(\lambda)} - (m+1), \;\; \lambda > 0. \tag{61}$$

The stochastic representation obtains now the form

$$\begin{aligned} u(x) &= \frac{g_m(k|x-\xi|)}{g_m(e_m)} E_{\text{ext}}^x \left[\frac{u(\check{X}_\tau)}{P_m(\cos(\check{\Theta}_\tau))} \right] + \frac{g_m(k|x-\xi|)}{g_m(k\eta)} E_{\text{int}}^x \left[\frac{u(\check{X}_\tau)}{P_m(\cos(\check{\Theta}_\tau))} \right] \\ &+ \frac{g_m(k|x-\xi|)}{P_m(\cos(\theta_{m+\gamma,1}))} E_{\text{lat}}^x \left[\frac{u(\check{X}_\tau)}{g_m(k|\check{Y}_\tau|)} \right], \; x \in \tilde{D}_m^{e,\gamma}(\xi) \end{aligned} \tag{62}$$

To reveal the special features of this representation, we need to explain its particular building. The selection of the parameters has a hierarchical structure. The cone $\tilde{D}_m^{e,\gamma}(\xi)$ defines the crucial dimensions η and $L = \frac{e_m}{k}$. Then the coefficient C_m in the definition formula of g_m is chosen such that the function g_m obtains the same values at the end points of its domain, i.e., $g_m(k\eta) = g_m(e_m)$. This means that

$$C_m = \frac{y_m(e_m) - y_m(k\eta)}{j_m(e_m) - j_m(k\eta)} \tag{63}$$

Then the coefficients $\frac{g_m(k|x-\xi|)}{g_m(e_m)}$ and $\frac{g_m(k|x-\xi|)}{g_m(k\eta)}$ of the first two terms of the Representation (62) are equal and the equipartition has arisen as a possibility. What remains is to ascertain that the probabilities of hitting the two cups are comparable. This can be realized if the point x is appropriately selected. To show the selection criterion for the observation point, let us examine the example pictured in Figure 4.

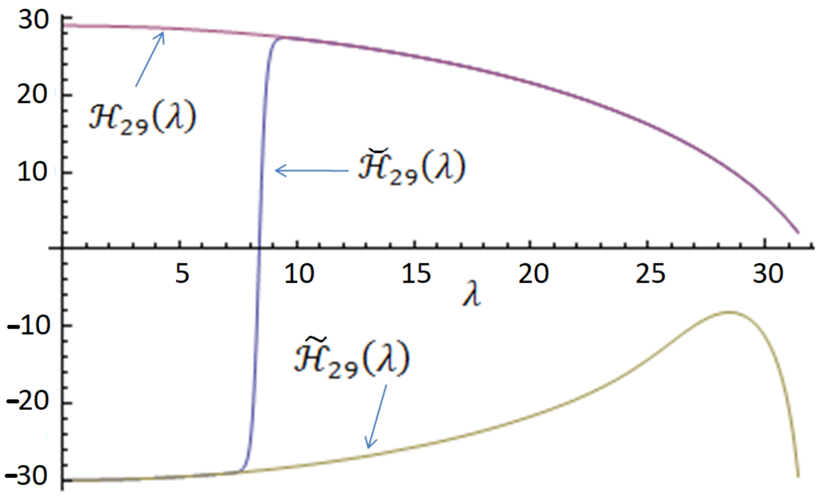

Figure 4. The driving terms of the three stochastic representations for $m = 29$. The geometrical parameters were selected as $k\eta = \pi$ and $e_{29} = 10\pi$. Then, according to the rule (63), the radial function g_{29} has the form $g_{29}(\lambda) = 1.41 \times 10^{25} j_{29}(\lambda) - y_{29}(\lambda)$.

We remark that the modified driving term $\breve{\mathcal{H}}_m(\lambda)$ is separated into two branches—each one coinciding with one of the driving terms of the older stochastic processes—plus an abrupt transition region from the one situation to the other. The function $\breve{\mathcal{H}}_m(\lambda)$ vanishes when $g_m'(\lambda)$ becomes zero, as implied by Equation (61). The imposed condition $g_m(k\eta) = g_m(e_m)$ and the specific monotonicity behavior of g_m in the interval $[k\eta, e_m]$ guarantee the existence of only one point λ_m where g_m' vanishes and simultaneously g_m takes its minimal value.

As a simple analysis reveals and Figure 5 demonstrates, the constituents $C_m j_m$ and $(-y_m)$ of g_m take the same value near the minimum point λ_m, i.e.,

$$C_m j_m(k|x-\xi|) = -y_m(k|x-\xi|) = \frac{1}{2} g_m(k|x-\xi|). \tag{64}$$

The unique point x, satisfying Equation (64), is selected to define the initial point x of the stochastic process. Every trajectory emanating from x is subjected, in the beginning of its travel, to a pure Brownian boost since the driving term is locally zero. So its initial directivity obeys the Brownian law, but once it finds an orientation, the driving term obtains abruptly one of the already studied inward or outward behaviors, pushing the trajectory to cross the corresponding cup. Intuitively, one half of the trajectories meets the exterior cup, while the other half escapes from the smaller inner spherical shell. This indication can be verified rigorously. Indeed, the above encountered probabilistic analysis applies again to define estimates of the hitting probabilities. Following the argumentation met in Proposition 4, using Equation (64) and the asymptotic analysis of the involved special functions, we find that

$$P^x\left[\left\{|Y_\tau| = \frac{e_m}{k}\right\}\right] \geq \breve{A}_m(x,\xi,\eta) := \frac{g_m(e_m)}{g_m(k|x-\xi|)} \frac{[j_{m+\gamma}(k|x-\xi|)y_{m+\gamma}(k\eta) - j_{m+\gamma}(k\eta)y_{m+\gamma}(k|x-\xi|)]}{[j_{m+\gamma}(e_m)y_{m+\gamma}(k\eta) - j_{m+\gamma}(k\eta)y_{m+\gamma}(e_m)]}$$
$$\approx \frac{C_m j_m(e_m)}{2C_m j_m(k|x-\xi|)} \frac{j_{m+\gamma}(k|x-\xi|)}{j_{m+\gamma}(e_m)} \underset{\gamma\to 0}{\to} \frac{1}{2} \tag{65}$$
$$P^x[\{|Y_\tau| = \eta\}] \geq \breve{B}_m(x,\xi,\eta) := \frac{g_m(k\eta)}{g_m(k|x-\xi|)} \frac{[j_{m+\gamma}(e_m)y_{m+\gamma}(k|x-\xi|) - j_{m+\gamma}(k|x-\xi|)y_{m+\gamma}(e_m)]}{[j_{m+\gamma}(e_m)y_{m+\gamma}(k\eta) - j_{m+\gamma}(k\eta)y_{m+\gamma}(e_m)]}$$
$$\approx \frac{(-y_m(k\eta))}{2(-y_m(k|x-\xi|))} \frac{y_{m+\gamma}(k|x-\xi|)}{y_{m+\gamma}(k\eta)} \underset{\gamma\to 0}{\to} \frac{1}{2} \tag{66}$$

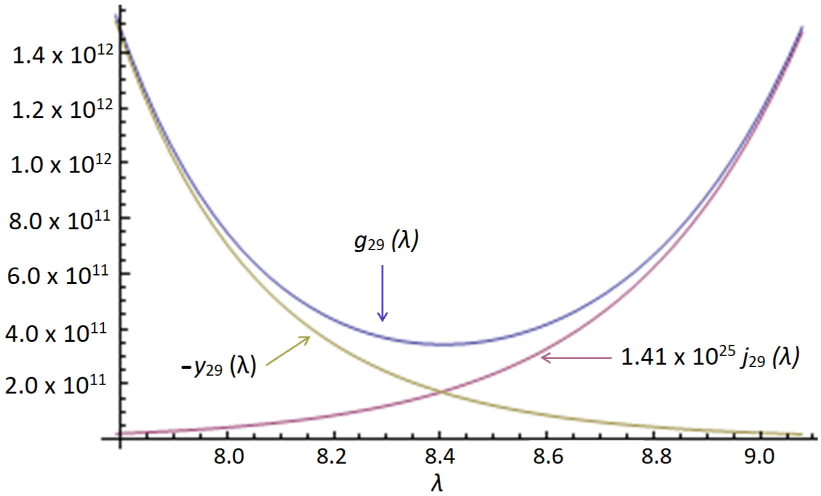

Figure 5. The function g_{29} and its constituent terms near the minimum point λ_{29}.

The design of the geometrical parameters involved in the third representation has been applied in a specific sequence, which will be proved useful in the framework of the inverse problem. As far as the direct problem is concerned, the reasonable hierarchy is a little bit different: The first concern is the selection of the observation point x and the next step is the determination of the coefficient C_m appearing in g_m by demanding the validity of relation $C_m j_m(k|x-\xi|) = -y_m(k|x-\xi|)$ (see Equation (64)). Then what remains is the determination of the interior and exterior radii η, $\frac{e_m}{k}$. These parameters could be selected arbitrarily but in that case the probabilities of escaping through the shells would be of different order and then the coefficients $\frac{g_m(k|x-\xi|)}{g_m(e_m)}$ and $\frac{g_m(k|x-\xi|)}{g_m(k\eta)}$ of Representation (62) would be unbalanced in order to compensate this unfitness. If equipartition of escaping is desired then the one parameter is selected freely and the other one must chosen (the selection is unique) so that $g_m(k\eta) = g_m(e_m)$. Additional criteria concerning the choice of the free parameters have numerical origin and will be presented in the next section.

Summarizing, the Representation (62) gives an equivalent role to the exterior and interior spherical shells since the involved coefficients are balanced to keep the same order while the probabilistic status favors the equipartition of the produced trajectories. The third lateral term is again predominated by the term $P_m^{\zeta-1}(\cos(\theta_{m+\gamma,1}))$, $\zeta > 1$ and fades away when $\gamma \to 0$. The Representation (62) is the conditionally probabilistic analogue of Green's integral representation in the direct scattering problem with the advantage of validity on cropped conical portions of the exterior space having as spherical cups subsets of the far field region and the scatterer's surface.

4. The Application Features of the Stochastic Implementation

The stochastic differential Equations (15) can be slightly modified on the basis of recurrent relations valid for spherical Bessel and Legendre functions, thus providing the discretized Euler scheme [15]

$$
\begin{aligned}
&Y_0 = (Y_0^{(1)}, Y_0^{(2)}, Y_0^{(3)}) = x \\
&Y_{n+1}^{(i)} = Y_n^{(i)} - \left[\frac{(2m+1)}{|Y_n|^2} Y_n^{(i)} - \frac{k Y_n^{(i)} j_{m-1}(k|Y_n|)}{|Y_n| j_m(k|Y_n|)}\right] \Delta t_n - \frac{P'_{m-1}(\cos\theta_n)}{P_m(\cos\theta_n)} \frac{1}{|Y_n|^2} Y_n^{(i)} \Delta t_n + \Delta B_n^{(i)}, \;\; i = 1,2 \\
&Y_{n+1}^{(3)} = Y_n^{(3)} - \left[\frac{(2m+1)}{|Y_n|^2} Y_n^{(3)} - \frac{k Y_n^{(3)} j_{m-1}(k|Y_n|)}{|Y_n| j_m(k|Y_n|)}\right] \Delta t_n + \frac{m P_{m-1}(\cos\theta_n)}{\cos\theta_n P_m(\cos\theta_n)} \frac{1}{|Y_n|^2} Y_n^{(3)} \Delta t_n + \Delta B_n^{(3)}.
\end{aligned} \tag{67}
$$

Similarly, the dual stochastic differential System (56) leads to the discretized scheme

$$
\begin{aligned}
&\widetilde{Y}_0 = (\widetilde{Y}_0^{(1)}, \widetilde{Y}_0^{(2)}, \widetilde{Y}_0^{(3)}) = x \\
&\widetilde{Y}_{n+1}^{(i)} = \widetilde{Y}_n^{(i)} - \left[\frac{(2m+1)}{|\widetilde{Y}_n|^2} \widetilde{Y}_n^{(i)} - \frac{k \widetilde{Y}_n^{(i)} y_{m-1}(k|\widetilde{Y}_n|)}{|\widetilde{Y}_n| y_m(k|\widetilde{Y}_n|)}\right] \Delta t_n - \frac{P'_{m-1}(\cos\theta_n)}{P_m(\cos\theta_n)} \frac{1}{|\widetilde{Y}_n|^2} \widetilde{Y}_n^{(i)} \Delta t_n + \Delta B_n^{(i)}, \;\; i = 1,2 \\
&\widetilde{Y}_{n+1}^{(3)} = \widetilde{Y}_n^{(3)} - \left[\frac{(2m+1)}{|\widetilde{Y}_n|^2} \widetilde{Y}_n^{(3)} - \frac{k \widetilde{Y}_n^{(3)} y_{m-1}(k|\widetilde{Y}_n|)}{|\widetilde{Y}_n| y_m(k|\widetilde{Y}_n|)}\right] \Delta t_n + \frac{m P_{m-1}(\cos\theta_n)}{\cos\theta_n P_m(\cos\theta_n)} \frac{1}{|\widetilde{Y}_n|^2} \widetilde{Y}_n^{(3)} \Delta t_n + \Delta B_n^{(3)}.
\end{aligned} \tag{68}
$$

Both Euler schemes (in [7], we presented an approach of higher accuracy leading to a stronger Taylor scheme inspired by [15], but this is not necessary in the framework developed herein) are sufficient in the case of relatively spacious cones and their comparison with the static case [7] reveals the influence of the wave number k. Examining first the Scheme (68), we see that when $k \to 0$, we take the stochastic framework encountered in [7]. Consequently, in the absence of k, the term $-\frac{(2m+1)}{|Y_n|^2} Y_n^{(i)}$ has the main contribution to radial driving of the stochastic process, representing mainly the attraction of the conical vertex ξ.

However, the situation changes drastically when handling the stochastic law (67). This can be easily conceived when $k|Y_n| \to 0$ and the asymptotic regime for the spherical Bessel functions is evoked. Then the term $\frac{(2m+1)}{|Y_n|^2} Y_n^{(i)} - \frac{k Y_n^{(i)} j_{m-1}(k|Y_n|)}{|Y_n| j_m(k|Y_n|)}$ tends to zero and the dominating factor in drift is $\frac{m P_{m-1}(\cos\theta_n)}{\cos\theta_n P_m(\cos\theta_n)} \frac{1}{|Y_n|^2} Y_n^{(3)} \Delta t_n$, forcing the trajectory to move upwards, as already predicted analytically in previous paragraphs. In addition, the terms $-\frac{P'_{m-1}(\cos\theta_n)}{P_m(\cos\theta_n)} \frac{1}{|Y_n|^2} Y_n^{(i)} \Delta t_n, \;\; i = 1,2$ do not allow the paths to move far away from the local z-axis.

The combined Scheme (60) merits its own attention, but, as already explained, the initial direction of the trajectory activates one of the possible branches (the outward or inward scheme) that have been described above. Actually, every numerical experiment is evolved with probability one half via the rule (67) or (68) exclusively, since going back in the opposite direction has a tremendously small likelihood.

Having in mind the remarks above, we focus on the first stochastic System (67) and investigate the geometric ingredients of the conical region $\tilde{D}_m^{e,\gamma}(\xi)$ where the Representation (55) applies. As far as the crucial parameter e_m, defining the height of the cone, is concerned, it is necessary that e_m is slightly less than the first local maximum point of j_m. To clarify this criterion, we present for example the case ($m = 8$) in Figure 6.

It is clear that only when e_8 is chosen to be less than the first maximum point $\lambda_{8,1} = 10.01$ of j_8, the driving term $\mathcal{H}_8$ remains positive in the whole interval $[0, e_8)$. To take advantage of all the available space, it is preferable to choose the parameter e_m to be less and close to the first maximum point $\lambda_{m,1}$ of j_m. In Table 1 we see some important cases which will emerge in the applications. It is noticed that the appeared height of the cones is the maximal possible for every particular m. Nevertheless, we have the flexibility to select smaller heights if this is useful.

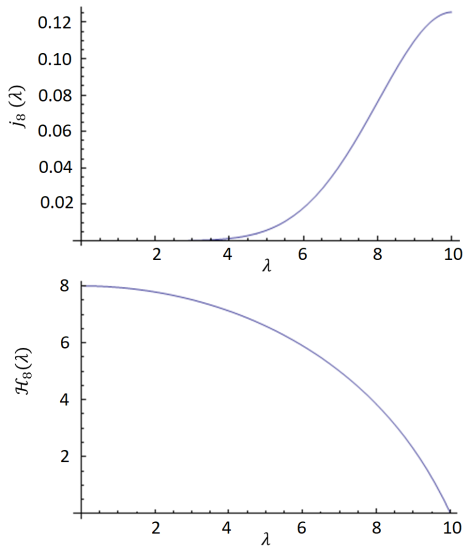

Figure 6. The decreasing positive function $\mathcal{H}_8(\lambda)$ and the subsequent spherical Bessel function $j_8(\lambda)$.

Table 1. Some characteristic cones for several values of the parameter m.

Parameter m Defining the Spherical Bessel j_m	The Maximal Height of the Cone $\frac{e_m}{k} = \frac{e_m}{2\pi}\lambda$
3	$\frac{\lambda}{2}$
4	$\frac{3\lambda}{4}$
5	λ
8	$\frac{3\lambda}{2}$
11	2λ
29	5λ

When m augments then the parameter e_m (the height of the cone) increases while the cone becomes narrower as the interior protective cone is defined by the angle $\theta_{m+\gamma,1} = \arccos(\chi_{m+\gamma,1})$, which is a decreasing sequence. The selection of the parameter η is based on the remark that in the beginning of the process, the driving term offers an axial boost $\frac{mP_{m-1}(\cos\theta_n)}{\cos\theta_n P_m(\cos\theta_n)}\frac{1}{|Y_n|^2}Y_n^{(3)}\Delta t_n|_{n=0} = \frac{m(x-\xi)}{|x-\xi|^2}\Delta t_0$, which becomes extremely large when x approaches ξ. Then if we are interesting in assigning rapid directivity to the outward orientation of the process, we are obliged to design a small distance $|x-\xi|$, a fact rendering even smaller the distance η. In most of the numerical experiments of the outwards orientated stochastic cluster, the reference selection $k\eta < 0.005\pi$ was adopted in connection with the choice $k|x-\xi| < 0.01\pi$. What remains is defining the parameter γ for every particular m. Referring to Equation (55), the second term $\frac{j_m(k|x-\xi|)}{j_m(k\eta)}E^x_{\text{int}}\left[\frac{u(X_\tau)}{P_m(\cos(\Theta_\tau))}\right]$ has a coefficient of order one thanks to the proximity of the arguments x, ξ and so this term is governed by the very small probability of first exit from the interior shell, being so suppressed. The first term $\frac{j_m(k|x-\xi|)}{j_m(e_m)}E^x_{\text{ext}}\left[\frac{u(X_\tau)}{P_m(\cos(\Theta_\tau))}\right]$ is strongly favored by the probabilistic law since the majority of the trajectories hit this cup. This term has apparently a generally small coefficient $\frac{j_m(k|x-\xi|)}{j_m(e_m)}$—due to the monotonicity of the Bessel function—but this just implies that the main contribution of the expectation is produced from strikes near the angle $\theta_{m+\gamma,1}$ where the denominator takes small values. It is important to determine γ in a normalization sense in order for the leading term of the representation to be implemented numerically efficiently. There are several good choices, as numerical experiments revealed, but the optimized one has an exponential structure. One convenient choice leading to a balanced representation, as will be verified later, consists in taking $\gamma = \gamma_\nu$ such that

$$P_m(\cos\theta_{m+\gamma_\nu,1}) = e^{-\frac{1}{e(\zeta-1)}\left(\frac{j_m(e_m)}{j_m(k|x-\xi|)}\right)^{\nu+2}}, \; \nu > \zeta - 2, \tag{69}$$

where we meet the parameter ζ introduced in Proposition 6. This is always possible since $P_m(\cos\theta_{m+\gamma,1}) \to 0$ monotonically as γ goes to zero. Then, the first leading term of Representation (55) is an expectation involving the field $u(x)$—over the exterior cup—with a multiplicative function $\left(\frac{j_m(k|x-\xi|)}{j_m(e_m)}\right)\frac{1}{P_m(\cos(\Theta_\tau))}$, which (as we move to the circular boundary of the cup) approaches the value $\left(\frac{j_m(k|x-\xi|)}{j_m(e_m)}\right)\frac{1}{P_m(\cos\theta_{m+\gamma_\nu,1})}$ that equals $\left(\frac{j_m(k|x-\xi|)}{j_m(e_m)}\right)e^{\frac{1}{e(\zeta-1)}\left(\frac{j_m(e_m)}{j_m(k|x-\xi|)}\right)^{\nu+2}}$, which is greater (it holds that $xe^{\frac{a}{x}} \geq ea, \forall x > 0$, when $a > 0$) than $\frac{1}{(\zeta-1)}\left(\frac{j_m(e_m)}{j_m(k|x-\xi|)}\right)^{\nu+1}$. Consequently, the greater the parameter ν, the stronger the weighting of the involvement of the marginal hitting points near the peripheral circle of the exterior cup. This has a parallel pace with the diminishing of the estimate expressing the contribution of the whole lateral conical surface. Indeed, evoking Proposition 6 (applied with $\gamma = \gamma_\nu$), the lateral term is bounded as follows:

$$\begin{aligned}
\frac{j_m(k|x-\xi|)}{P_m(\cos(\theta_{m+\gamma,1}))}\left|E^x_{\text{lat}}\left[\frac{u(X_\tau)}{j_m(k|Y_\tau|)}\right]\right| \quad &\leq \quad C\frac{j_m(k|x-\xi|)}{j_m(k\eta)}e^{\frac{k^2\zeta}{2}T}\left(\frac{j_m(e_m)}{j_m(k|x-\xi|)}\right)^{\zeta}P_m^{\zeta-1}(\cos(\theta_{m+\gamma,1})) \\
&\leq \quad C'e^{\frac{k^2\zeta}{2}T}\left(\frac{j_m(e_m)}{j_m(k|x-\xi|)}\right)^{\zeta}e^{-\frac{1}{e}\left(\frac{j_m(e_m)}{j_m(k|x-\xi|)}\right)^{\nu+2}} && (70) \\
&<< \quad C'e^{\frac{k^2\zeta}{2}T}\left(\frac{j_m(k|x-\xi|)}{j_m(e_m)}\right)^{\nu+2-\zeta}, \; \nu > \zeta - 2. && (71)
\end{aligned}$$

The discussion above offers some a priori analytical origin to the selection criteria of the several involved parameters, whose final choice obeys of course the specific characteristics of the separate particular cases encountered in next sections.

5. On Exploiting the Remote Field via Stochastic Analysis in the Service of the Inverse Scattering Problem

In this section it will be demonstrated how the far field information is transferred on the surface of a sphere C_R enclosing the space that is occupied by the scatterer and belonging to the regime of the near field. This sphere is centered at the coordinate origin O, has radius R and could be the circumscribing sphere of the scatterer. If the scatterer is a convex structure then the sphere could be replaced by the surface ∂D of the scatterer itself and this is a special and interesting case that merits separate treatment and is presented in the forthcoming subsection.

The goal is to transfer the data given in the far field region on the surface of the sphere C_R. What is offered as data is the far field pattern or equivalently the Dirichlet to Neumann operator (for some possible selections of the directivity $\hat{k}$ of the incident wave) in a large sphere with radius R_L equal to a few wavelengths. Focusing on a specific orientation $\hat{x}_1$, the distance $R_L - R$ has to be interpreted as the height L of a cone K_1, having as axis this orientation and as vertex the uniquely determined point ξ_1 of the sphere C_R (see Figure 7).

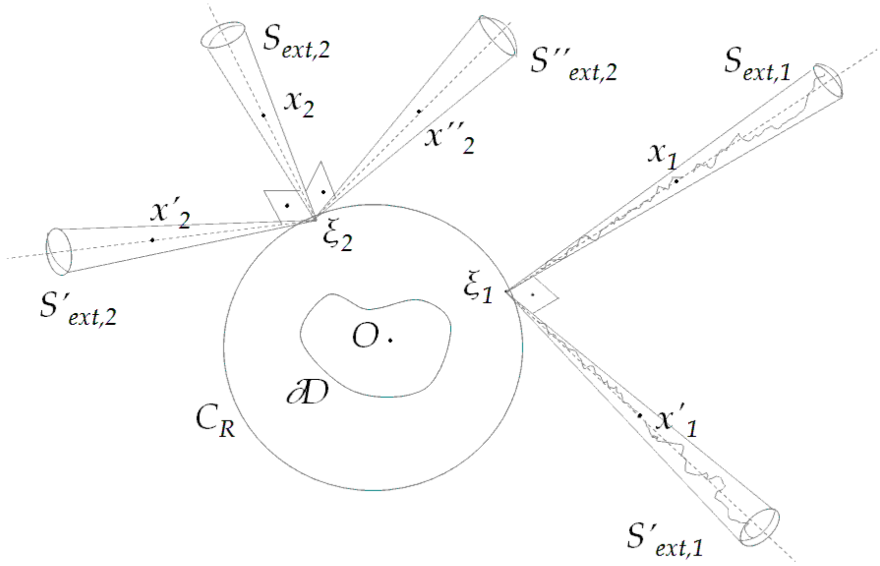

Figure 7. Transferring data from the far field to the near field region.

This selection gives birth to the dimensionless quantity kL, which must be fitted with the appropriate parameter e_m discussed earlier. In other words, we have to select the appropriate order m such that kL is slightly smaller than the first maximum point of j_m. The interior cup of the cone is selected via the choice of the parameter η, which as discussed in the previous section is assigned a considerably small value for several reasons. Then we construct the appropriate combination $g_m = C_m j_m - y_m$, by selecting C_m via the rule (63), assuring that g_m obtains the same values at the upper and lower cups of the cone ($g_m(k\eta) = g_m(e_m)$). Given the parameter m, the angle of the cone is defined uniquely and equals $\theta_{m+\gamma_\nu,1}$. Then the starting point x_1 of the stochastic process is selected according to the Formula (64). We recall that this choice establishes the equipartition of spreading of trajectories towards the cups of the conical structure. We proceed then to the solution of the stochastic differential System (60) in combination with Equation (61) and the starting condition $\check{Y}_0 = x_1 - \xi_1$. As discussed above, every numerical experiment obeying to the aforementioned stochastic law, splits with probability $\frac{1}{2}$ to one of the dual numerical Schemes (67) and (68) presented in Section 4. The crucial point though is that Formula (62) is adequate to apply not to the physical field u but to the vector field $M(\check{X}_t) = (\check{X}_t - x_1) \times \nabla u(\check{X}_t)$. First, this is legitimate since the field M belongs to the kernel of the Helmholtz operator. It is actually reminiscent of one of the three respectively perpendicular Navier eigenvectors constructed on the basis of a scalar solution of the Helmholtz equation, via repeated suitable application of the curl operator. Secondly, it is an efficient choice since M constitutes a null field at the point x_1. This annihilation leaves active in the stochastic representation only the contributions of the field on the spherical walls of the conical structure. On the basis of the equipartition property $g_m(k\eta) = g_m(e_m)$ and Relation (70), the Equation (62) becomes

$$
\begin{aligned}
0 &= M(x_1) = \frac{g_m(k|x_1-\xi_1|)}{g_m(e_m)} E^{x_1}_{\text{ext}}\left[\frac{M(\check{X}_\tau)}{P_m(\cos(\check{\Theta}_\tau))}\right] + \frac{g_m(k|x_1-\xi_1|)}{g_m(k\eta)} E^{x_1}_{\text{int}}\left[\frac{M(\check{X}_\tau)}{P_m(\cos(\check{\Theta}_\tau))}\right] \\
&+ \frac{g_m(k|x_1-\xi_1|)}{P_m(\cos(\theta_{m+\gamma,1}))} E^{x_1}_{\text{lat}}\left[\frac{M(\check{X}_\tau)}{g_m(k|\check{Y}_\tau|)}\right] \Rightarrow \\
0 &= \frac{g_m(k|x_1-\xi_1|)}{g_m(e_m)}\left[E^{x_1}_{\text{ext}}\left[\frac{M(\check{X}_\tau)}{P_m(\cos(\check{\Theta}_\tau))}\right] + E^{x_1}_{\text{int}}\left[\frac{M(\check{X}_\tau)}{P_m(\cos(\check{\Theta}_\tau))}\right]\right] + \\
&\quad O\left(e^{\frac{k^2\zeta}{2}T}\left(\frac{j_m(e_m)}{j_m(k|x-\xi|)}\right)^{\zeta} e^{-\frac{1}{e}\left(\frac{j_m(e_m)}{j_m(k|x-\xi|)}\right)^{\nu+2}}\right),\ \nu > \zeta - 2. \Rightarrow
\end{aligned}
$$

$$E_{\mathrm{ext}}^{x_1}\left[\frac{M(\breve{X}_\tau)}{P_m(\cos(\breve{\Theta}_\tau))}\right]+E_{\mathrm{int}}^{x_1}\left[\frac{M(\breve{X}_\tau)}{P_m(\cos(\breve{\Theta}_\tau))}\right]=O\left(e^{\frac{k^2\zeta}{2}T}\left(\frac{j_m(e_m)}{j_m(k|x-\xi|)}\right)^{\zeta+1}e^{-\frac{1}{e}\left(\frac{j_m(e_m)}{j_m(k|x_1-\xi_1|)}\right)^{\nu+2}}\right),\ \nu>\zeta-2.$$

For large ν (which affects slightly but effectively γ_ν and the cone via its angle) the right hand side of the last equation fades away exponentially. In addition, given that $k\eta << 1$, the interior cup is shrunk and the expectation value over it behaves as $E_{\mathrm{int}}^{x}\left[\frac{M(\breve{X}_\tau)}{P_m(\cos(\breve{\Theta}_\tau))}\right]\approx -y_1\times\nabla u(\xi_1)E_{\mathrm{int}}^{x}\left[\frac{1}{P_m(\cos(\breve{\Theta}_\tau))}\right]$, where $y_1=x_1-\xi_1$. So we obtain what is a simple but one of the fundamental results of this work:

$$\hat{y}_1\times\nabla u(\xi_1)=\frac{1}{|x_1-\xi_1|E_{\mathrm{int}}^{x_1}\left[\frac{1}{P_m(\cos(\breve{\Theta}_\tau))}\right]}E_{\mathrm{ext}}^{x_1}\left[\frac{(\breve{X}_\tau-x_1)\times\nabla u(\breve{X}_\tau)}{P_m(\cos(\breve{\Theta}_\tau))}\right], \tag{72}$$

expressing the tangential derivative $\nabla_S u$ over the the sphere C_R at the point ξ_1. Then knowing ∇u (this is not identical to the information offered by the far field pattern but strongly related to that. It is of course reminiscent of the gathered information offered by the Dirichlet to Neumann operator for a specific wave number and a concrete direction of incidence. See Remark 2) on the suitable portion of the far field region leads to the determination of the tangential derivative of the field on the—potentially–circumscribing sphere of the scatterer. If we are interested in determining fully the gradient of u in ξ_1, we need to repeat the process above via the implication of a cone K_1' with the same vertex ξ_1, vertical axis normal to the axis of K_1 and identical geometrical parameters. This process incorporates a new set of numerical stochastic experiments concerning now the stochastic process $\breve{X}_t'$ involves data on a different portion of the remote region (see Figure 7) and provides that

$$\hat{y}_1'\times\nabla u(\xi_1)=\frac{1}{|x_1'-\xi_1|E_{\mathrm{int}}^{x_1'}\left[\frac{1}{P_m(\cos(\breve{\Theta}_\tau'))}\right]}E_{\mathrm{ext}}^{x_1'}\left[\frac{(\breve{X}_\tau'-x_1')\times\nabla u(\breve{X}_\tau')}{P_m(\cos(\breve{\Theta}_\tau'))}\right], \tag{73}$$

where $\hat{y}_1'$ is normal to $\hat{y}_1$ and $|x_1'-\xi_1|=|x_1-\xi_1|$. Determining thus $\hat{y}_1\times\nabla u(\xi_1)$ and $\hat{y}_1'\times\nabla u(\xi_1)$ implies reconstruction of the full vector field $\nabla u(\xi_1)$. The last assertion holds even in the case that the surrounding surface is not spherical and so the vector $\hat{y}_1$ is not necessarily the normal vector on the surface. The same situation can be repeated for every arbitrary point ξ_2 located on C_R. The selection of the secondary perpendicular cone is arbitrary and depends on the availability of data (see Figure 7).

Combining Equations (72) and (73), suppressing indices, setting $\hat{y}''=\hat{y}\times\hat{y}'$ and exploiting the identical geometric characteristics of the cones, we easily prove that

$$\begin{aligned}\nabla u(\xi)=\frac{1}{|x-\xi|E_{\mathrm{int}}^{x}\left[\frac{1}{P_m(\cos(\breve{\Theta}_\tau))}\right]}&\left[(\hat{y}'\hat{y}''-\hat{y}''\hat{y}')\cdot E_{S_{\mathrm{ext},x}}^{x}\left[\frac{(\breve{X}_\tau'-x)\times\nabla u(\breve{X}_\tau)}{P_m(\cos(\breve{\Theta}_\tau))}\right]\right.\\ &\left.-\hat{y}\hat{y}''\cdot E_{S_{\mathrm{ext},x'}}^{x'}\left[\frac{(\breve{X}_\tau'-x')\times\nabla u(\breve{X}_\tau')}{P_m(\cos(\breve{\Theta}_\tau'))}\right]\right].\end{aligned} \tag{74}$$

In fact, it is not always necessary to use a different set of cones (and far field subregions) for every particular point ξ of the surrounding near field surface. This remark can be explained in a converse manner introducing the well known case of the restricted far field data. The question is to determine the range of influence of this restricted set. Indeed, let us assume that the vector ∇u is measured on a portion S_0 of the remote field regime. As depicted in Figure 8, the surface element S_0 defines a truncated cone S_{tr} which divides the surface C_R into two parts, the shadowed one and its complement C_R^+, on which a grid of points ξ_i can be distributed.

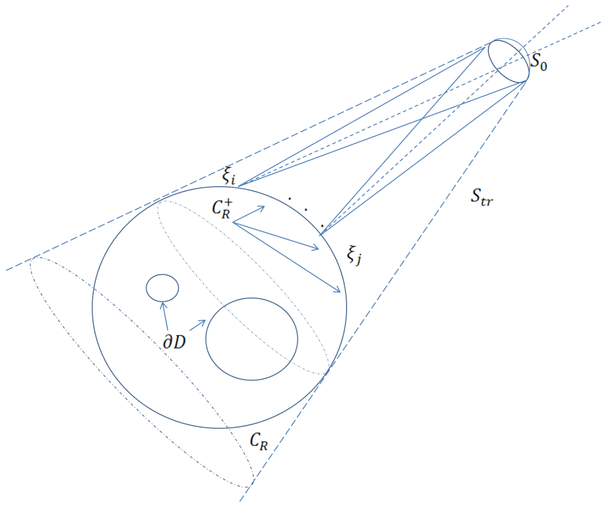

Figure 8. The region of influence of the data confined on S_0.

Every such point constitutes the vertex of a cone whose base is the sub-surface S_0. These cones do not have—in their majority—upper spherical cups orientated with their axis $\hat{y}_i$, but this geometrical slight declination does not affect the probabilistic setting developed so far given that the influence of the bases to the evolution of the trajectories applies only to the final steps of their travel. In summary, if only $\hat{y}_i \times \nabla u(\xi_i)$ are to be determined (for a plethora of points ξ_i, $i = 1, 2, ..., N$ on C_R^+), then the information on S_0 is enough. Moreover, if we are interested in determining the vectors $\nabla u(\xi_i)$ themselves, we evoke the dual perpendicular cones (as demonstrated in Figure 7) whose base assembly forms a supplementary far field data region of indispensable utility.

The method will be accomplished after the determination of u itself on C_R is fulfilled. We consider the—perpendicular to M—vector solution of the Helmholtz equation $N(x;\alpha) = \nabla \times M(x)|_{x_i=\alpha}$. It is easily proved that the scalar field $v(x;\alpha) := (x-\alpha) \cdot N(x;\alpha) = 2(x-\alpha)\cdot\nabla u(x) + (x-\alpha)(x-\alpha) : \nabla\nabla u(x) + k^2|x-\alpha|^2 u(x)$ belongs also to the kernel of the Helmholtz operator and is annihilated clearly at the point α. Let us, for example, pay attention to the stochastic Representation (62) in connection with the conical structures with vertex point ξ_2 of Figure 7. We take into account three mutually vertical cones K_2, K_2', K_2'' (geometrically identical) and apply Equation (62) to the Helmholtz equation solutions $v(x;x_2), v(x;x_2')$ and $v(x;x_2'')$, respectively. We obtain then

$$v(\xi_2;\alpha) = -\frac{1}{E^{\alpha}_{\text{int}}\left[\frac{1}{P_m(\cos(\check{\Theta}^{(\alpha)}_{\tau}))}\right]} E^{\alpha}_{\text{ext}}\left[\frac{v(\check{X}^{(\alpha)}_{\tau};\alpha)}{P_m(\cos(\check{\Theta}^{(\alpha)}_{\tau}))}\right], \text{ for } \alpha = x_2, x_2' \text{ and } x_2'' \tag{75}$$

In the far field regime $|x| \to \infty$ and especially on the three surface portions $S_{\text{ext},2}, S'_{\text{ext},2}, S''_{\text{ext},2}$, the field $v(x;\alpha)$ has the asymptotic behavior $v(x;\alpha) \approx 2x \cdot \nabla u(x) + xx : \nabla\nabla u(x) + k^2|x|^2 u(x) = -\mathbb{B}u(x)$, where we meet the well known Beltrami operator $\mathbb{B}$. In Remark 2, we investigate the characteristics of the function $F_1(x) = \mathbb{B}u(x)$ and its mining mechanism from the offered data.

We proceed by adding the Relations (75) for $\alpha = x_2, x_2'$ and x_2''. The left hand side of the produced equation is proved to be equal to $-2|x_2-\xi_2|(\hat{y}_2+\hat{y}_2'+\hat{y}_2'')\cdot\nabla u(\xi_2) + |x_2-\xi_2|^2\Delta u(\xi_2) + 3k^2|x_2-\xi_2|^2 u(\xi_2) = -2|x_2-\xi_2|(\hat{y}_2+\hat{y}_2'+\hat{y}_2'')\cdot\nabla u(\xi_2) + 2k^2|x_2-\xi_2|^2 u(\xi_2)$, if we take into account that u satisfies the Helmholtz equation. Taking the interior expectations to be identical and suppressing subscripts (referring to a generic point ξ), we obtain

$$-2|x-\xi|(\hat{y}+\hat{y}'+\hat{y}'')\cdot\nabla u(\xi)+2k^2|x-\xi|^2u(\xi)=\frac{\sum_{\alpha\in\{x,x',x''\}}E^{\alpha}_{S_{\mathrm{ext},\alpha}}\left[\frac{F_1(\check{X}^{(\alpha)}_\tau)}{P_m(\cos(\check{\Theta}^{(\alpha)}_\tau))}\right]}{E^{x}_{\mathrm{int}}\left[\frac{1}{P_m(\cos(\check{\Theta}^{(x)}_\tau))}\right]}.$$

Exploiting Equation (74), we find

$$\begin{aligned}u(\xi) &= \frac{1}{2k^2|x-\xi|^2E^{x}_{\mathrm{int}}\left[\frac{1}{P_m(\cos(\check{\Theta}^{(x)}_\tau))}\right]}\left\{\sum_{\alpha\in\{x,x',x''\}}E^{\alpha}_{S_{\mathrm{ext},\alpha}}\left[\frac{F_1(\check{X}^{(\alpha)}_\tau)}{P_m(\cos(\check{\Theta}^{(\alpha)}_\tau))}\right]\right.\\ &+ \left.(\hat{y}''-\hat{y}')\cdot E^{x}_{S_{\mathrm{ext},x}}\left[\frac{(\check{X}^{(x)}_\tau-x)\times\nabla u(\check{X}^{(x)}_\tau)}{P_m(\cos(\check{\Theta}^{(x)}_\tau))}\right]-\hat{y}''\cdot E^{x'}_{S_{\mathrm{ext},x'}}\left[\frac{(\check{X}^{(x')}_\tau-x')\times\nabla u(\check{X}^{(x')}_\tau)}{P_m(\cos(\check{\Theta}^{(x')}_\tau))}\right]\right\}\end{aligned} \tag{76}$$

which constitutes one of the basic results of this work.

Remark 2. *The scattered field $u(X)=u(X;\hat{k},k)$, obeys the Atkinson–Wilcox expansion [11]*

$$u(X)=\frac{e^{ik|X|}}{|X|}\sum_{n=0}^{\infty}\frac{f_n(\hat{X};\hat{k},k)}{|X|^n} \tag{77}$$

outside the circumscribing sphere ($|X|>R$), where we encounter the radiation pattern $f_0(\hat{X};\hat{k},k)=u_\infty(\hat{X};\hat{k},k)$, which appeared in Equation (4). In second order approximation, we have the following asymptotic form for the remote field:

$$u(X)=\frac{e^{ik|X|}}{|X|}\left[f_0(\hat{X};\hat{k},k)+\frac{1}{|X|}f_1(\hat{X};\hat{k},k)\right]+u_2(X),\quad |X|^2u_2(X)\to 0,\ \text{as}\ |X|\to\infty \tag{78}$$

The coefficients f_n are related via the well known [11] recursion scheme $2iknf_n=n(n-1)f_{n-1}+\mathbb{B}f_{n-1}$, $n=1,2,\ldots$. So the field $F_1(X)=\mathbb{B}u(X)$ that appeared in the Representation (76) is expressed as

$$F_1(X)=\mathbb{B}u(X)=\frac{e^{ik|X|}}{|X|}\mathbb{B}f_0(\hat{X};\hat{k},k)+O(\frac{1}{|X|^2})=\frac{e^{ik|X|}}{|X|}2ikf_1(\hat{X};\hat{k},k)+O(\frac{1}{|X|^2})\ \text{as}\ |X|\to\infty, \tag{79}$$

involving thus the second order approximation f_1 of the remote field expansion. The direct detection of f_1 in measurements via (78) is complicated and demanding since it requires high sensitivity analysis and suffers from the implication of measurement errors. However, its determination via a posteriori analysis of data is straightforward: The far field pattern always has expansion in terms of the spherical harmonics Y_n^m

$$f_0=\sum_{n=0}^{\infty}\sum_{m=-n}^{n}b_n^mY_n^m,\ \text{with coefficients}\ b_n^m=\int_\Omega f_0(\hat{X})\overline{Y_n^m}(\hat{X})d\hat{X}. \tag{80}$$

(Ω stands for the unit sphere). Theoretically, in the absence of noise, the coefficients b_n^m rapidly decay, satisfying [16] the growth condition $\sum_{n=0}^{\infty}\left(\frac{2n}{keR}\right)^{2n}\sum_{m=-n}^{n}|b_n^m|^2<\infty$. In practice, the coefficients b_n^m are calculated via the integrals that appeared in (80) on the basis of the measured far field and then an expansion of the possibly polluted pattern f_0 in terms of spherical harmonics (see again (80)) can be constructed. Due to noise, the expansion coefficients of f_0 could violate the aforementioned growth condition but generally maintain a rapidly decreasing behavior.

Thus, the field $2ikf_1=\mathbb{B}f_0$ is represented as the expansion $2ikf_1=-\sum_{n=0}^{\infty}n(n+1)\sum_{m=-n}^{n}b_n^mY_n^m$, taking into consideration the fact that the spherical harmonics Y_n^m are the eigenfunctions of the Beltrami operator $\mathbb{B}$ ($\mathbb{B}Y_n^m=-n(n+1)Y_n^m$). The last expansion represents a stable estimation of f_1 in the case that the noise corruption does not alter the before-mentioned growth behavior to such an extent that the reasonable and much weaker summability condition $\sum_{n=0}^{\infty}n^2(n+1)^2\sum_{m=-n}^{n}|b_n^m|^2<\infty$ is violated.

The same process is followed to construct numerical implementations of the remote vector wave field $(X-x)\times\nabla u(X)$, participating in the expectations that appeared in representations (74) and (76). Indeed, in the case that the starting point x of the stochastic process is designed to belong to the near field region and especially close to the vertex ξ, the function $(X-x)\times\nabla u(X)$ behaves like $\frac{e^{ik|X|}}{|X|}\hat{X}\times\mathbb{D}f_0(\hat{X})$ as $|X|\to\infty$, where we recognize the spherical surface tangential gradient $\mathbb{D}=\hat{\theta}\frac{\partial}{\partial\theta}+\frac{1}{\sin\theta}\frac{\partial}{\partial\phi}$. Evoking the spherical harmonic expansion of the far field pattern, we find that

$$
\begin{aligned}
(X-x)\times\nabla u(X) &\approx \frac{e^{ik|X|}}{|X|}\hat{X}\times\mathbb{D}f_0(\hat{X}) = \frac{e^{ik|X|}}{|X|}\hat{X}\times\sum_{n=0}^{\infty}\sum_{m=-n}^{n} b_n^m\mathbb{D}Y_n^m(\hat{X}) \\
&= -\frac{e^{ik|X|}}{|X|}\sum_{n=0}^{\infty}\sum_{m=-n}^{n}\sqrt{n(n+1)}b_n^m\mathbb{C}_n^m(\hat{X}),\ |X|\to\infty,
\end{aligned}
\tag{81}
$$

where there emerges, for every pair (n,m), one of the Hansen mutually orthogonal vector spherical harmonics (i.e., the eigenvectors $\mathbb{P}_n^m(\hat{X})=\hat{X}Y_n^m(\hat{X})$, $\mathbb{B}_n^m(\hat{X})=\frac{1}{\sqrt{n(n+1)}}\mathbb{D}Y_n^m(\hat{X})$ and $\mathbb{C}_n^m(\hat{X})=\frac{1}{\sqrt{n(n+1)}}\mathbb{D}Y_n^m(\hat{X})\times\hat{X}$).

The final step of the method is to implement the Representations (74) and(76) by evoking Monte Carlo simulations of the emerged expectation values over the spherical cups. Thus, for every cone under consideration we perform N repetitions of independent stochastic experiments, providing trajectories obeying the stochastic differential System (60). These trajectories are gathered and special attention is paid to their traces over the exterior and interior surfaces of the cones. On these exit points, we calculate the contribution of the involved fields, which are present in the expectation arguments and take appropriately the mean values of the accumulated terms. Consequently, Representation (76) acquires the numerical implementation

$$
\begin{aligned}
u(\xi) &= \frac{1}{2k^2|x-\xi|^2\sum_{j=1}^{N_{\text{int}}^{(x)}}\left[\frac{1}{P_m(\cos(\breve{\Theta}_j^{(x)}))}\right]}\left\{\sum_{\alpha\in\{x,x',x''\}}\sum_{i=1}^{N_{\text{ext}}^{(\alpha)}}\left[\frac{F_1(\breve{X}_i^{(\alpha)})}{P_m(\cos(\breve{\Theta}_i^{(\alpha)}))}\right]\right. \\
&+ \left.(\hat{y}''-\hat{y}')\cdot\sum_{i=1}^{N_{\text{ext}}^{(x)}}\left[\frac{(\breve{X}_i^{(x)}-x)\times\nabla u(\breve{X}_i^{(x)})}{P_m(\cos(\breve{\Theta}_i^{(x)}))}\right]-\hat{y}''\cdot\sum_{i=1}^{N_{\text{ext}}^{(x')}}\left[\frac{(\breve{X}_i^{(x')}-x')\times\nabla u(\breve{X}_i^{(x')})}{P_m(\cos(\breve{\Theta}_i^{(x')}))}\right]\right\},
\end{aligned}
\tag{82}
$$

where $N_{\text{ext}}^{(\alpha)}$ represents the number of exits of the trajectories through the exterior surface of the cone K^{α}. Given that the involved cones in Representation (76) are identical, then $N_{\text{ext}}^{(x)}=N_{\text{ext}}^{(x')}=N_{\text{ext}}^{(x'')}$. In addition, the theoretically established equipartition of the trajectories, pertaining to their orientation, implies that $N_{\text{ext}}^{(x)}\approx N_{\text{int}}^{(x)}\approx\frac{N}{2}$, a fact which is approved by the experiments.

On Reconstructing Convex Scatterers

We consider in this section the pilot case of convex scatterers. As discussed above, the developed analysis of transferring data from the remote region to the near field region can take place up to the surface of the scatterer given that it is feasible to exploit a system of cones which do not intersect portions of the scattering bodies. Then, the surface ∂D is an assembly of all the points ξ_i, $i=1,2,..$ on which the right hand side of Equation (76) equals $-e^{ik\hat{k}\cdot\xi_i}$, satisfying thus the boundary condition (2). The motif is to reveal that only one direction of excitation is sufficient to provide adequate inversions, and so the case $\hat{k}=-\frac{1}{\sqrt{3}}(1,1,1)$ will be examined uniformly for all the case studies.

In the beginning, we consider the primitive case of a spherical scatterer of radius a, centered at the coordinate origin. Being more specific, we consider the simple case of $a=1$

and $k = 2$ ($\lambda = \pi$ length units). The needed synthetic data are produced via the well known representations [16] of the scattering field and the far field pattern:

$$u(x) = \sum_{n=0}^{\infty} \sum_{m=-n}^{n} a_n^m h_n^{(1)}(k|x|) Y_n^m(\hat{x}) \text{ and } f_0(\hat{x}) = \frac{1}{k} \sum_{n=0}^{\infty} \frac{1}{i^{n+1}} \sum_{m=-n}^{n} a_n^m Y_n^m(\hat{x}) \text{ with } a_n^m = -4\pi i^n \frac{j_n(ka)}{h_n^{(1)}(ka)} Y_n^m(\hat{k}).$$

So, the terms b_n^m, representing the spherical harmonic expansion coefficients of the far field pattern are equal to $b_n^m = 4\pi i \frac{j_n(ka)}{h_n^{(1)}(ka)} Y_n^m(\hat{k})$ and play an important role to the construction of the arguments of the forthcoming numerically simulated expectation terms involved in the functions $\tilde{u}(\xi_i)$, $i = 1, 2, ...M$, denoting the right hand side of Equation (76) for several points ξ_i, sampled uniformly inside a cube $\mathcal{Q}$ centered at the coordinate origin and having edges of length $2\lambda = \frac{4\pi}{k} = 2\pi$. This cube hosts the determinable scatterer. We consider a remote distance $|X|$ of order of $5\lambda = \frac{10\pi}{k} = 5\pi$ where the synthetic data are collected. We focus on the portion of data that is confined on a spherical subregion of the sphere $k|X| = 10\pi$ around the radial direction $\hat{r}_0 = -\hat{k} = \frac{1}{\sqrt{3}}(1, 1, 1)$. The aforementioned choices define the crucial geometric parameter $k|X| = e_m = 10\pi$, defining the range of the remote scattering field and the typical size of the involved cones. So, according to the parametric analysis described in previous sections, the integer m takes the optimal value $m = 29$. The abovementioned range of used data S_0 (on the sphere $k|X| = 10\pi$ and in the vicinity of $\hat{r}_0$) has a spherical polar aperture confined by the angle $\theta_{29,1}$. (We recall that the supplementary data introduced by the dual perpendicular cones of type K' and K'' play also a crucial role). The vertex of every involved cone K_i is one of the sampling points ξ_i; its interior cup is very close to the vertex via the selection $k\eta = 0.01\pi$, which leads to a concrete Helmholtz kernel $g_{29} = C_{29} j_{29} - y_{29} = 1.29 \times 10^{85} j_{29} - y_{29}$ so that the equilibrium $g_{29}(k\eta) = g_{29}(e_{29})$ is established. This description defines the typical geometrical characteristics of the involved cones so that the interrelation between the remote and near field region is exploitable. Using again the parametric analysis exposed previously, the starting point x_i of every individual stochastic process taking place inside K_i should belong to the axis of the cone and distances from the vertex of a specific length so that the equipartition of the directivity of the trajectories is ensured (see Relation (64)). Then, the geometrical feature $k|x_i - \xi_i|$ for the involved cones, is determined to have the exact value 0.2524π. The hitting probabilities are theoretically foreseen by Equations (65) and (66) to be $P^x\left[\{|Y_\tau| = \frac{e_m}{k}\}\right] \geq 0.500039$ and $P^x[\{|Y_\tau| = \eta\}] \geq 0.499774$ and the simulations verified this prediction.

Prescribing further the performed numerical experiments, it is noticed that inside the cube $\mathcal{Q}$, a set of $M = 20^3$ uniformly distributed potentially candidate surface points ξ_i has been sampled and for every $i \in \{1, 2, ..., M\}$, stochastic experiments have been performed pertaining to the solution of the underlying stochastic differential equations in the cones K_i, K_i' and K_i''. If additional a priori information was given about the possible location of the interface ∂D, the distribution of the sampling points ξ_i would have selective characteristics. In any case, the Monte Carlo realization of the involved expectation terms required at most $N = 10^2$ experiments—repetitions with a typical life time of traveling inside the cones expressed via the rule $k^2 T = 10^{-2}$. This result is in conjunction with the uniform selection of the parameters $\zeta = 2$ and $\nu = 1$, defining in detail the angle of the cones according to the results of Section 4. This stochastic implementation led to the determination of the stochastic terms $\tilde{u}(\xi_i)$, $i \in \{1, 2, ..., M\}$, expressing, as mentioned before, the right hand side of Expression (76).

The inversion algorithm consists in constructing and investigating the objective function $G(\xi) = |\tilde{u}(\xi) + e^{ik\hat{k}\cdot\xi}|$. The points ξ_i assigning small values to the functional $G(\xi_i)$ are the supporting points of the surface ∂D. In Figure 9, we plot the level set of the interpolating function $G(\xi)$, representing the set of points satisfying the criterion $G(\xi) = \epsilon$ with $\epsilon \leq 10^{-2}$.

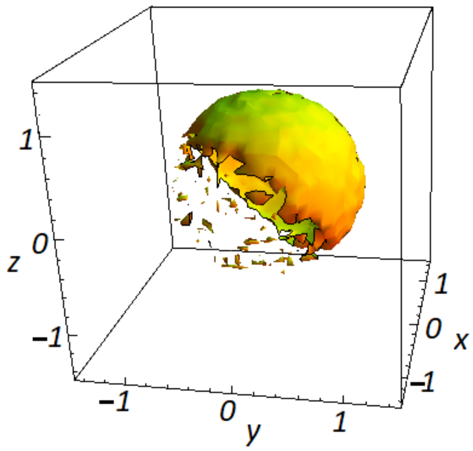

Figure 9. The reconstruction of the sphere of radius $a = 1$, in the framework of the backscattering case $\hat{r}_0 = -\hat{k} = \frac{1}{\sqrt{3}}(1,1,1)$. The principal data are distributed over a surface element of measure $2\pi(5\pi)^2(1 - \cos\theta_{29,1})$ and are supplemented with additional information over the dual cones of type K' and K''.

We verify the high level of accuracy in the reconstruction as far as the region of influence of S_0 is concerned (Figure 8). It is reasonable that the points ξ_i belonging to the shadowed region cannot be reconstructed appropriately, since they pertain to cones intersecting the scatterer and occupying regions, part of which do not belong to the real scattering region. Actually this is the drawback when non-convex scatterers are investigated since the stochastic representation has been formulated on the assumption that the trajectories are free to move in subregions where the underlying Helmholtz differential equation is valid. (In this case, we reach similarly the circumscribing sphere and proceed further differently as will be clarified in the next section)

The presented methodology has been applied also in the case of the inverse acoustic problem by the ellipsoidal surface $\frac{x^2}{a_1^2} + \frac{y^2}{a_2^2} + \frac{z^2}{a_3^2}$ with considerably unequal semi-axes $a_1 = 4, a_2 = 3, a_3 = 2$. In order to avoid the complexity of the ellipsoidal harmonics [17] and to open up the rich and simple arsenal of data of the direct problem in the realm of the low-frequency region, we consider the indicative case $k = \frac{1}{5}$ and evoke the stable results encountered in [18] and the developed methodology in [19]. More precisely, the far field pattern acquires the form

$$\begin{aligned} f_0(\hat{x};\hat{k},k) = &-\frac{1}{I^0} + ik\left(\frac{1}{I^0}\right)^2 + k^2\left(\frac{1}{I^0}\right)^3\left\{1 - \frac{(I^0)^2}{3}\sum_{i=1}^3 a_n^2 + \frac{I^0}{3}\sum_{i=1}^3 a_n^4 I_n^1 - \frac{(I^0)^3}{3}\sum_{i=1}^3 \frac{\hat{x}_n\hat{k}_n}{I_n^1}\right. \\ &\left.+\frac{(I^0)^2}{6}\sum_{i=1}^3(\hat{x}_n^2 + \hat{k}_n^2)a_n^2\right\} - ik^3\left(\frac{1}{I^0}\right)^4\left\{1 - \frac{5}{9}(I^0)^2\sum_{i=1}^3 a_n^2 + \frac{2}{3}I^0\sum_{i=1}^3 a_n^4 I_n^1 + \frac{(I^0)^2}{6}\sum_{i=1}^3(\hat{x}_n^2 + \hat{k}_n^2)a_n^2\right\} \\ &+O(k^4), \end{aligned} \tag{83}$$

where the well known [18] elliptic integrals I^0 and I_n^1, $n = 1,2,3$ are involved.

Insisting on the back scattering setting $\hat{r}_0 = -\hat{k} = \frac{1}{\sqrt{3}}(1,1,1)$, we use (83) to furnish the necessary data appeared in the mean-value terms of Formula (82) exactly as we did in the spherical case. The 3D contour plot of the objective function $G(\xi) = \epsilon$ with $\epsilon \leq 10^{-2}$ gives the very accurate reconstruction depicted in Figure 10. The only difference in the parametric setting is that we have adopted a denser grid of sampling points ($M = 10^6$) to reveal the strong anisotropy of the scatterer.

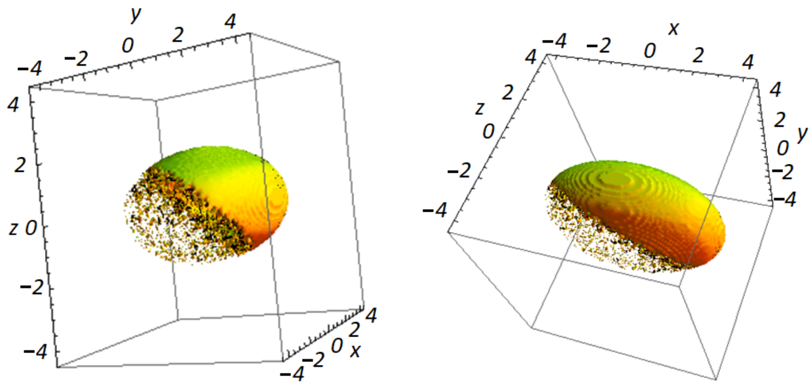

Figure 10. The reconstruction of the ellipsoidal surface $\frac{x^2}{16} + \frac{y^2}{9} + \frac{z^2}{4} = 1$, for one specific incidence $\hat{k} = -\frac{1}{\sqrt{3}}(1,1,1)$ and wave number $k = \frac{1}{5}$.

6. The Development and Implementation of the Inversion Method on the Basis of Near Field Measurements

6.1. Testing the Validity of the Stochastic Representation in Point-Source Radiation Processes

Focusing on developing a stochastic treatment of the near scattered field, we first present a very indicative case concerning the determination of radiating fields generated from point sources. So let us refer instantly to a radiating process not obeying the boundary value problem (1)–(3), but referring to the emanation of an outgoing acoustic from a multipole located at a point source. For example, we consider the azimuthally uniform radiating field $u_m(x;\xi) = h_m^{(1)}(k|x-\xi|)P_m(\cos\theta) = (j_m(k|x-\xi|) + iy_m(k|x-\xi|))P_m(\cos\theta)$ generated (we recognize, [20], the spherical Hankel function $h_m^{(1)}(k|x-\xi|)$) by a point source located at the point ξ. Adopting as the suitably adapted hosting conical region the one pertaining to the parameter m and having as vertex the point source ξ, we are in a position to verify analytically the Representation (55) or equivalently the equipartitioned stochastic Formula (62). Indeed, on the basis of the right hand side of Equation (55), we obtain easily the following result:

$$u(x;\xi) = u^{\text{ext}}(x;\xi) + u^{\text{int}}(x;\xi) := \frac{j_m(k|x-\xi|)}{j_m(e_m)} h_m^{(1)}(e_m) P^x\left[|Y_\tau| = \frac{e_m}{k}\right] + \frac{j_m(k|x-\xi|)}{j_m(k\eta)} h_m^{(1)}(k\eta) P^x[|Y_\tau| = \eta].$$

This is an exact result since the lateral term is equal to zero due to the elimination of the Legendre polynomial in the denominator of this term. Evoking the asymptotic results of Proposition 4, we find that the right hand side of last equation provides

$$h_m^{(1)}(e_m)\frac{j_{m+\gamma}(k|x-\xi|)}{j_{m+\gamma}(e_m)} + h_m^{(1)}(k\eta)\frac{y_{m+\gamma}(k|x-\xi|)}{y_{m+\gamma}(k\eta)} \underset{\gamma\to 0}{\to} j_m(k|x-\xi|) + i\, y_m(k|x-\xi|) = h_m^{(1)}(k|x-\xi|),$$

which in fact ascertains that the left hand side of (55) coincides with the value of the multipole radiating field at the point x. These remarks are verified also numerically: We select, for example, the cone corresponding to $m = 11$ with vertex ξ and $e_{11} = 4\pi$ (see Table 1). Our intention is to apply the stochastic Scheme (15) (and its numerical replica (67)) pertaining to the outwards orientated process, in the realm of which the correlation between the parameters x, η and ξ is not so restrictive any more (only the combined equi-partitioned stochastic process used in the far field regime is demanding for the relative selection of the geometric parameters). However, given that we are interested in examining the combined equipartitioned stochastic scheme as well making a fruitful comparison, we keep a common treatment concerning the criteria of selection of the geometrical characteristics and we choose methodological $k\eta = 5\pi \times 10^{-6}$ and $k|x-\xi| = 0.002676$. The expectations over the spherical cups are facilitated by the polar independence of the arguments leading to multiples of the pure probabilities that can be estimated analytically as before or calculated numerically via stochastic experiments. Taking advantage of this simple framework and exploiting the tabulated very accurate values of special functions, we reach to the very extreme but exact values $u^{\text{ext}} = (1.59344 - i\,1.10278) \times 10^{-40}$ and $u^{\text{int}} \approx 0 - i\,1.01964 \times 10^{41}$. Consequently, the sum $u^{\text{ext}} + u^{\text{int}}$ is in complete agreement with the value of $h_m^{(1)}(k|x - \xi|) = 1.59345 \times 10^{-40} - i\,1.01964 \times 10^{41}$ representing the assignment of the field at the point x. This result is presented along with similar cases pertaining to different cones presented in Table 2 that were adopted. The situation was repeated in cases where the stochastic Scheme (60) was with the stochastic Representation (62) for all the cases depicted in Table 2. The results are identical but the process was simplified due to the theoretically predicted equipartition of hitting probabilities and the stabilizing factor of the equipartition of the coefficients $\frac{g_m(k|x-\xi|)}{g_m(e_m)}$ and $\frac{g_m(k|x-\xi|)}{g_m(k\eta)}$, a fact that prevents from introducing different scale contributions of the participants of the stochastic representation. The aim of this presentation is to reveal the efficiency of the method in extreme cases, not being necessarily indicative of the scattering problem under investigation but enclosing special features of "tough" wave radiation, where strongly singular and regular terms coexist. In obstacle scattering processes the scattered field has of course a smoother behavior.

The situation becomes more demanding when the hosting cone and the involved multipole-type radiating solution correspond to different parameters m. Then the expectation values are θ dependent and the stochastic numerical experiments are indispensable. Working, for example, with the cone K_{11} and considering the outgoing radiating solution $u_9(x;\xi) = h_9^{(1)}(k|x - \xi|)P_9(\cos\theta)$, the probabilistic terms $E_Q^x\left[\frac{P_9(\cos(\breve{\Theta}_\tau))}{P_{11}(\cos(\breve{\Theta}_\tau))}\right]$, $Q \in \{\text{ext, int}\}$ emerge, whose determination requires the stochastic implementation by performing Monte Carlo experiments. For completeness reasons, we mention that in this particular case, it turns out that $u^{\text{ext}} = 1.07551 \times 10^{-32} + i\,7.64773 \times 10^{-33}$ and $u^{\text{int}} = 4.3198 \times 10^{-94} - i\,1.83044 \times 10^{33}$ and the produced sum is indeed equal to the outgoing field $h_9^{(1)}(k|x - \xi|)$ for $k|x - \xi| = 0.002676$.

Table 2. Validation of the Representation (55) in the case of radiating fields emanating from ξ. In all cases, $k\eta = \pi \times 10^{-6}$, while e_m take the prescribed values presented in Table 1.

m	$k\|x-\xi\|$	$h_m^{(1)}(k\|x-\xi\|)$	u^{ext}	u^{int}
3	0.000705	$3.337 \times 10^{-12} - i\,6.072 \times 10^{13}$	$(3.337 - i\,9.155) \times 10^{-12}$	$9.097 \times 10^{-31} - i\,6.072 \times 10^{13}$
4	0.003775	$2.149 \times 10^{-13} - i\,1.3696 \times 10^{14}$	$(2.149 - i\,2.9552) \times 10^{-13}$	$8.036 \times 10^{-35} - i\,1.3696 \times 10^{14}$
5	0.001346	$4.25 \times 10^{-19} - i\,1.589 \times 10^{20}$	$(4.25 - i\,3.19) \times 10^{-19}$	$2.324 \times 10^{-51} - i\,1.589 \times 10^{20}$
11	0.002676	$1.593 \times 10^{-40} - i\,1.0196 \times 10^{41}$	$(1.593 - i\,1.103) \times 10^{-40}$	$7.6 \times 10^{-115} - i\,1.0196 \times 10^{41}$

6.2. On Reconstructing Stochastically Star Shaped or Disconnected Scatterers via near Field Data

The aim of this section is the application of the aforementioned stochastic algorithm to the reconstruction of the scatterer on the basis of exploiting data offered on a spherical surface S_c which might coincide with or be broader than the circumscribing sphere of the scatterer. The concept is to take advantage of the data provided on S_c and reconstruct suitably the scattered field inside the ball B_c confined by S_c and hosting the scatterer. In fact, the portion $\tilde{S}$ of the spherical surface S_c, whose information is instantly utilized, constitutes the base of a cone $\tilde{K}$, whose vertex is orientated inside the ball B_c and consists in one of the domains—frequently encountered in this work—of the stochastic experiments. The broadness of the cone depends on its pervasiveness inside the ball B_c. The narrower the cone, the larger its potential maximal height and consequently its depth inside the matrix enclosing the scatterer. There is an intrinsic behavior reminiscent of the uncertainty principle between the width and height of the emerged cones. All this description refers to the parameters e_m and $\theta_{m,1}$ that are oppositely monotone with respect to the integer m, nominating the class of every particular cone. To clarify theses remarks, let us refer for simplicity to a particular case, where the sphere S_c is centered at the coordinate origin, has radius $R = 2\lambda$ and surrounds a scatterer with surface ∂D, as depicted in Figure 11.

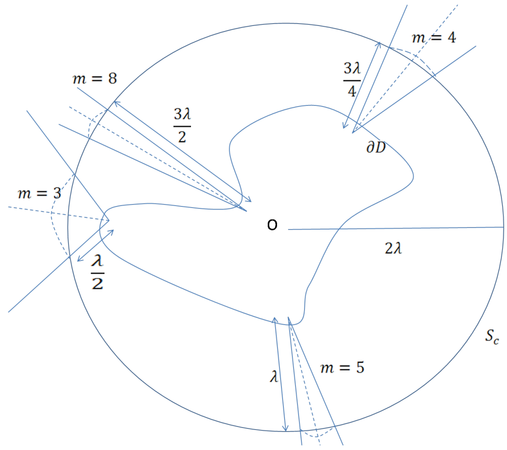

Figure 11. Every cone has a height that cannot exceed $\frac{e_m}{k} = \frac{e_m}{2\pi}\lambda$. For several parameters m, the taller versions of the corresponding cones are presented.

Some favorable cases are demonstrated, which have already be mentioned and tabulated in Table 1. For example, to explore detection to a depth of order $\frac{3\lambda}{4}$, the parameter m must be selected as equal or greater to the critical value $M_{\frac{3\lambda}{4}} = 4$. The intersection $\tilde{S}_m$ of every cone with the data surface S_c is slightly deformed compared with the original spherical upper cup of the cone, but, in every case, lies inside the genuinely constructed cone, accelerating thus the escape of the driven trajectories via the exterior cup. In Section 6.1, we tested the outgoing and equipartitioned stochastic models, on the basis of establishing reconstructions of the field values at the point x in relation with the traces of the stochastic trajectories on the exit cups. This has to be rescheduled when the reconstruction of the scatterer itself is sought. In fact, the intermediate point x is useful to be considered as a "blind" point similar to the far field pattern treatment. More precisely, we select the function $(X - x) \times \nabla u(X)$ to be subjected to stochastic analysis having in mind that it vanishes at the auxiliary point x. Applying the modified two-directional stochastic law (61), we take again Formula (72), which is rewritten slightly differently, taking into account a stricter treatment of the interior cup contribution and paying attention to the explicit reference to the incidence direction:

$$\hat{y} \times \nabla u(\tilde{\xi};\hat{k}) = \frac{1}{|x-\xi| E^x_{\text{int}}\left[\frac{1}{P_m(\cos(\breve{\Theta}_\tau))}\right]} E^x_{\tilde{S}_m}\left[\frac{(\breve{X}_\tau - x) \times \nabla u(\breve{X}_\tau;\hat{k})}{P_m(\cos(\breve{\Theta}_\tau))}\right] := k\mathcal{M}_m(\tilde{\xi};\hat{k}), \quad (84)$$

with $y = y_\xi = x - \xi$ and $\tilde{\xi} = \xi + \eta\hat{y}$. It is worthwhile to notice here that the incidence $\hat{k}$ is taken perpendicular to the axis $\hat{y}$ of the cone.

The point $\tilde{\xi}$ will be tested as a candidate scatterer's surface point and then the decomposition $\nabla u(\tilde{\xi}) = \hat{n}\frac{\partial u}{\partial n}(\tilde{\xi}) + (\mathbb{I} - \hat{n}\hat{n}) \cdot \nabla u(\tilde{\xi})$ will be used, where the normal vector $\hat{n}$ on the scatterer is unknown. In cases where $\tilde{\xi}$ lies on the surface ∂D, the boundary condition can be evoked, leading to

$$\hat{y} \times \nabla u(\tilde{\xi};\hat{k}) = \hat{y} \times \hat{n}\left(\frac{\partial u}{\partial n}(\tilde{\xi};\hat{k}) + i\hat{n} \cdot (k\hat{k})e^{ik\hat{k}\cdot\tilde{\xi}}\right) - i\hat{y} \times k\hat{k}e^{ik\hat{k}\cdot\tilde{\xi}} \quad (85)$$

Taking the complex conjugate of this equation, we obtain

$$\hat{y} \times \overline{\nabla u\ (\tilde{\xi};\hat{k})} = \hat{y} \times \hat{n}\left(\overline{\frac{\partial u}{\partial n}}(\tilde{\xi};\hat{k}) - i\hat{n} \cdot (k\hat{k})e^{-ik\hat{k}\cdot\tilde{\xi}}\right) + i\hat{y} \times k\hat{k}e^{-ik\hat{k}\cdot\tilde{\xi}} \quad (86)$$

Clearly the function $\overline{u}$ is an ingoing wave that cannot satisfy the Sommerfeld radiation Condition (3). We consider now the boundary value Problem (1)–(3) corresponding to the opposite incidence $(-\hat{k})$ having the outgoing solution $u(x;-\hat{k})$. Clearly, it holds that

$$\hat{y} \times \nabla u(\tilde{\xi};-\hat{k}) = \hat{y} \times \hat{n}\left(\frac{\partial u}{\partial n}(\tilde{\xi};-\hat{k}) - i\hat{n}\cdot(k\hat{k})e^{-ik\hat{k}\cdot\tilde{\xi}}\right) + i\hat{y} \times k\hat{k}e^{-ik\hat{k}\cdot\tilde{\xi}} \tag{87}$$

Substracting the last two equations we find that

$$\hat{y} \times \overline{\nabla u(\tilde{\xi};\hat{k})} - \hat{y} \times \nabla u(\tilde{\xi};-\hat{k}) = \hat{y} \times \hat{n}\left(\overline{\frac{\partial u}{\partial n}(\tilde{\xi};\hat{k})} - \frac{\partial u}{\partial n}(\tilde{\xi};-\hat{k})\right). \tag{88}$$

The left hand side of this relation (in the most probable case that it is not vanishing (We will examine separately the vanishing case)) can be constructed on the basis of Formula (84) applied twice for incidences $\hat{k}$ and $(-\hat{k})$. Consequently, the direction $\hat{t} = \hat{t}_{\xi} = \frac{\hat{y}\times\hat{n}}{|\hat{y}\times\hat{n}|}$ can be reconstructed, even if $t = |\hat{y} \times \hat{n}|$ is unknown. Projecting Equation (85) onto the vector $\hat{y} \times \hat{t}$, we obtain

$$\frac{1}{k}(\hat{y} \times \hat{t}) \cdot \left(\hat{y} \times \nabla u(\tilde{\xi};\hat{k})\right) = \hat{t} \cdot \nabla u(\tilde{\xi};\hat{k}) = -i\hat{t} \cdot \hat{k}e^{ik\hat{k}\cdot\tilde{\xi}}. \tag{89}$$

What remains to be discussed is what happens when the left hand side of Equation (88) vanishes. Actually, the difference $\left(\overline{\frac{\partial u}{\partial n}(\tilde{\xi};\hat{k})} - \frac{\partial u}{\partial n}(\tilde{\xi};-\hat{k})\right)$ cannot be zero on a portion of the scatterer's surface ∂D_0 with a non-zero measure. Indeed, in that case, the field $w(X) := \overline{u(X;\hat{k})} - u(X;-\hat{k})$ would satisfy the Helmholtz equation, asymptotic decaying behavior for large distances and zero Cauchy data on the portion ∂D_0 of the surface. This would imply that the field $w(x)$ is globally zero and this is a contradiction since an outgoing field cannot be identically equal to an ingoing acoustic field. Then, vanishing of the sides of Equation (88) implies that the normal unit vector $\hat{n}$ is parallel to the axis of the cone $\hat{y}$, which is a very accidental but well accepted result, offering information about the curvature of the scatterer at the point ξ. Returning to Equation (85), we see that it obtains the simplified form

$$\frac{1}{k}(\hat{y} \times \hat{k}) \cdot (\hat{y} \times \nabla u(\tilde{\xi};\hat{k})) = \frac{1}{k}\hat{k} \cdot \nabla u(\tilde{\xi};\hat{k}) = -ie^{ik\hat{k}\cdot\tilde{\xi}}. \tag{90}$$

We define

$$\hat{a}_{\xi} = \begin{cases} \hat{t}_{\xi} \text{ if } \overline{\mathcal{M}_m(\tilde{\xi};\hat{k})} \neq \mathcal{M}_m(\tilde{\xi};-\hat{k}) \\ \hat{k} \text{ if } \overline{\mathcal{M}_m(\tilde{\xi};\hat{k})} = \mathcal{M}_m(\tilde{\xi};-\hat{k}) \end{cases} \tag{91}$$

and so we are in a position to group the Results (89) and (90) by constructing the target function

$$\mathcal{L}_m(\xi) = \left|\frac{1}{k|x-\xi|E^x_{\text{int}}\left[\frac{1}{P_m(\cos(\breve{\Theta}_\tau))}\right]}E^x_{\breve{S}_m}\left[\frac{[(\hat{y}_{\xi}\cdot(\breve{X}_\tau - x))\hat{a}_{\xi} - (\hat{a}_{\xi}\cdot(\breve{X}_\tau - x))\hat{y}_{\xi}]\cdot\nabla u(\breve{X}_\tau;\hat{k})}{P_m(\cos(\breve{\Theta}_\tau))}\right] + i\hat{a}_{\xi}\cdot\hat{k}e^{ik\hat{k}\cdot\tilde{\xi}}\right|. \tag{92}$$

The function $\mathcal{L}_m(\xi)$ theoretically vanishes when the point $\tilde{\xi}$, located very close to the vertex ξ, belongs to the surface ∂D. So imposing the constraint $\mathcal{L}(\xi) = \epsilon$, with $\epsilon << 1$ and sampling over a grid of candidate surface points ξ_i, $i = 1, 2, ..., M$ leads to the construction of level sets describing the surface of the scatterer.

The sampling process depends on a priori information concerning generic geometric characteristics of the inclusions under reconstruction. For example, if we are given a star shaped scatterer ∂D, described by the polar representation ($\mathbb{S}^2$ stands for the unit sphere) $r\hat{r} = f(\hat{r})\hat{r}$, $\hat{r} \in \mathbb{S}^2$ then the structure of the sampling grid has a radial architecture. More precisely, the vertex ξ of the conical region moves with a preselected step length towards the coordinate origin O over the half line connecting O with the employed portion of the spherical surface S_c, defining thus a concrete direction $\hat{r}$. Using different surface patches involves separate radial semi-axes and directions $\hat{r}$. Every position of the slipping down sampling point ξ defines a critical parameter m, characterizing the wider possible conical surface that can be employed to apply the method, and corresponds to one specific implementation of the stochastic algorithm, leading to the determination of the value of the function $\mathcal{L}_m(\xi)$. The first time this value coincides with a small threshold $\epsilon = .01$ terminates the descent on the line $\hat{r}$ and provides the unique point $f(\hat{r})\hat{r}$ of the scatterer. The situation is visualized in Figure 12, where the reconstruction of a cubic scatterer of semi-edges 2, $\sqrt{3}$, $\sqrt{2}$ length units (in x, y, z direction, respectively) is performed. The synthetic data are provided in the realm of low-frequency regime and are borrowed by the methodology described in [21] (and the references cited therein [22,23]), where the implication of data noise is intrinsically investigated. The exploited data belong to the depicted circumscribing sphere of radius 5 length units. The wave number λ is equal to 2.5 units so that a complete geometric correspondence with Figure 11 is guaranteed.

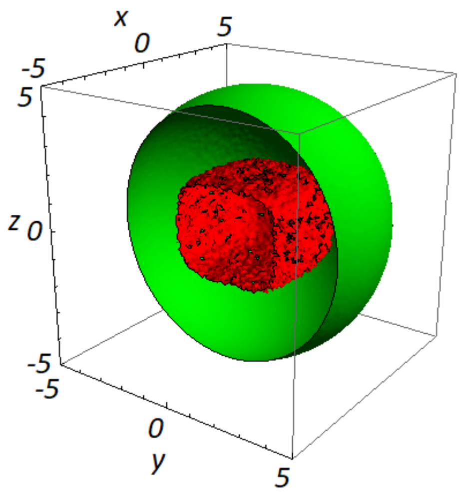

Figure 12. The reconstruction of the surface of the cubic scatterer with semi-edges 2, $\sqrt{3}$, $\sqrt{2}$ length units in cartesian coordinates. To reveal transparently the structure of the inversion, the region $x > -1.8$ has been illustrated.

The disconnected case (multiple scattering problem) requires a uniform sampling of vertices ξ_i, i = 1, 2, ..., M inside the orthogonal parallelepiped with axes of lengths 4, 2, 2 along the cartesian axes x, y, z, respectively, enclosing the scattering objects, in the same manner as in the far field inversion regime encountered in previous section. For the sake of simplicity, we expose just the inversion of two spheres with centers located on the x-axis (positions $x_1 = -1$ and $x_2 = 2$) and radii $a_1 = \sqrt{0.5}$ and $a_2 = 1$, respectively. The synthetic data are produced via the implication of the bispherical coordinate system and the analysis presented in [24] similarly to the treatment implemented in the introductory work [7]. Two separate cases are considered as far as the richness of the data is concerned. In the first case, the data are limited and offered on two spherical portions of the circumscribing sphere, as shown in Figure 13, while the second case refers to complete set of data on S_c. In real situations, the targets are unknown and so the selection of these spherical shells cannot be prescheduled. However, this concrete selection has been adopted intentionally since it represents the less informative scenario (the poorest data pool) given that the gap between the spheres is totally shadowed by the scatterers. The reconstruction in both cases presented in Figure 13 is well indicative as far as the potential of the stochastic inversion is concerned.

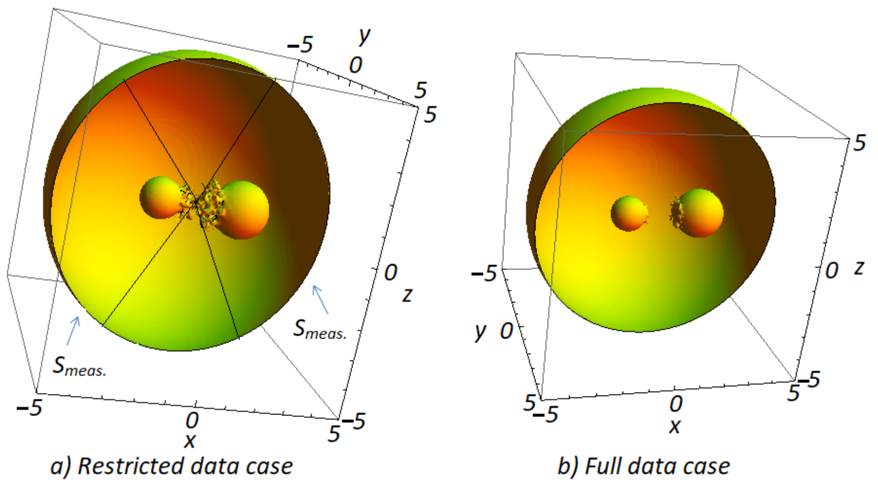

Figure 13. Reconstruction for the disconnected scatterer case: Detecting two spheres with radii equal to 1 and $\frac{1}{\sqrt{2}}$ centered at the points $x = 2$ and $x = -1$ of the x-axis, respectively.

The algorithm described in this section could be used as well in the realm of far field measurements in the case of convex star-shaped scatterers. Indeed, the alternative to detour the implication of additional measurement sets on the dual conical surfaces presented in Section 5 emerges via the current implementation. Comparing the approaches, their particular ingredients are revealed. The dual cones approach is based on one specific excitation $\hat{k}$ and three perpendicular cones providing data on three separate conical spherical cups in the far field regime. In addition, special treatment of the data is required to construct the field $F_1(\check{X}_\tau^{(\alpha)})$ that appeared in Representation (76). In contrast, the methodology of this section involves measurements generated by two opposite incidence directions $\hat{k}$ and $(-\hat{k})$ every time but restricted on the exterior cup of a single cone for every particular group of Monte Carlo stochastic experiments. Moreover, there is no need to interfere with the spherical harmonic expansion of the acoustic field any more in order to construct the auxiliary field F_1. Phenomenically, the second method seems privileged but a more attentive examination reveals some intrinsic special properties. First the incidence direction $\hat{k}$ must be perpendicular to the direction $x - \xi$, which could be demanding in a far field experimental setting, at the same time that the first approach does not impose such kinds of limitations. Secondly, in every realization of the second approach, the quantitative criterion (91) has to be examined, defining every time the very next choice (92). While this repeated "if" structure of the second algorithm does not impose some essential numerical burden, the first approach is totally free of any intrinsic geometric constraint.

7. Conclusions

The direct and inverse acoustic scattering problems, in the time-reduced form, are investigated in this work, in the realm of a novel probabilistic approach. The general methodological framework is the construction of stochastic processes emanating from the observation point and hitting efficiently the boundaries hosting surface conditions and measurements. These stochastic processes carry hidden information for the geometrical and physical characteristics of the scattering problem. Three alternative stochastic representations for the scattering field are constructed and investigated throughout the work, involving stochastic process with outgoing, ingoing and equipartitioned orientation. The domain of mobility of the trajectories is designed to be minimal and confined strictly by the scatterer, the data region and narrow lateral repellent conical surfaces, influencing drastically the directivity of the stochastic experiments.

The great advantage of this design is that only cropped sub-regions of the exterior space are used to settle connections between restricted data and narrow portions of the unknown scatterer. Thus, the reconstruction acquires an effective locality, reminiscent of the privileges, encountered in high frequency regime or geometric optics. However, this locality gain, developed herein, is not due to the measure of the stimulating frequency but owes its appearance to the multiple conditions applied to the probabilistic law, governing the underlying stochastic processes. In brief terms, selecting the singular points (attractive or repellent) of the cones and the subsequent repellent conical surfaces is a multi-parametric geometric design, simulating a conical wave-guide forcing the trajectories to evolve, mimicking acoustic rays.

Special attention has been paid to the inverse scattering problem with separate treatment of the far field and near field data cases. The reconstruction of the surface of the scatterer (either connected or disconnected) has been proved exact and optimal even in the case of restricted data. In the authors' opinion, the theoretical design and numerical fulfilment of the stochastic investigation pertaining to the inverse acoustic scattering problem, and developed in the current work, has a primitive novelty among techniques with similar purposes. That is why there exists the belief that this work initiates the perspective of handling more general exterior elliptic boundary value problems in unbounded domains via the conditioned probabilistic approach, proposed herein.

Author Contributions: Conceptualization, A.C.; Data curation, A.C. and L.G.; Formal Analysis, A.C.; Investigation, A.C., L.G. and E.V.; Methodology, A.C. and E.V.; Project administration, A.C.; Software, L.G. and A.C.; Validation, A.C. and E.V.; Writing—original draft preparation, A.C. and E.V. All authors have read and agreed to the published version of the manuscript.

Funding: This research received no external funding.

Institutional Review Board Statement: Not applicable.

Informed Consent Statement: Not applicable.

Data Availability Statement: Not applicable.

Conflicts of Interest: The authors declare no conflict of interest.

References

1. Rayleigh, L. On James Bernoulli's theorem in probabilities. *Philos. Mag.* **1899**, *47*, 246–251. [CrossRef]
2. Courant, R.; Friedrichs, K.; Lewy H. Uber die partiellen differenzen gleichungen der mathematischen Physik. *Math. Ann.* **1928**, *100*, 32–74. [CrossRef]
3. Chati, K.M.; Grigoriu, D.M.; Kulkarni, S.S.; Mukherjee, S. Random walk method for the two- and three-dimensional Laplace, Poisson and Helmholtz′s equations. *Int. J. Numer. Meth. Eng.* **2001**, *51*, 1133–1156. [CrossRef]
4. Oksendal, B. *Stochastic Differential Equations, An Introduction with Applications*, 6th ed.; Springer: Berlin/Heidelberg, Germany, 2003.
5. Lamperti, J. *Stochastic Properties, A Survey of the Mathematical Theory*, 1st ed.; Springer: New York, NY, USA, 1977.
6. Papanikolaou, C.G.; Keller, B.J. Stochastic Differential Equations with Applications to Random Harmonic Oscillators and Wave Propagation in Random Media. *SIAM J. Appl. Math.* **1971**, *21*, 287–305. [CrossRef]
7. Charalambopoulos, A.; Gergidis, N.L. A novel stochastic method for the solution of direct and inverse exterior elliptic problems. *Q. Appl. Math.* **2018**, *76*, 65–111. [CrossRef]
8. Tusheng, Z. Probabilistic Approach to the Neumann problem. *Acta Math. Appl. Sin.* **1990**, *6*, 126–134.
9. Hsu, P. Probabilistic Approach to the Neumann Problem. *Commun. Pure Appl. Math.* **1985**, *38*, 445–472. [CrossRef]
10. Bass, F.R.; Hsu, P. Some Potential Theory for Reflecting Brownian Motion in Holder and Lipschitz Domains. *Ann. Probab.* **1991**, *19*, 486–508. [CrossRef]
11. Wilcox, H.C. A generalization of theorems of Rellich and Atkinson *Proc. Amer. Math. Soc.* **1956**, *7*, 271–276. [CrossRef]
12. Ihlenburg, F. *Finite Element Analysis of Acoustic Scattering, Applied Mathematical Sciences*, 1st ed.; Springer: New York, NY, USA, 1998; Volume 132.
13. Iaskov, V. *Inverse Problems for Partial Differential Equations, Applied Mathematical Sciences*, 3rd ed.; Springer: Cham, Switzerland, 2017; Volume 127.
14. Zapala, M.A. Jensenâ€™s Inequality for Conditional Expectations in Banach Spaces. *Real Anal. Exch.* **2000**, *26*, 541–552. [CrossRef]
15. Kloeden, E.P.; Platen, E.; Schurz, H. *Numerical Solution of SDE Through Computer Experiments*, 3rd ed.; Springer: Berlin, Germany, 2003.
16. Colton, D.; Kress, R. *Inverse Acoustic and Electromagnetic Scattering Theory, Applied Mathematical Sciences*, 2nd ed.; Springer: Berlin/Heildeberg, Germany, 1998; Volume 93.
17. Dassios, G. *Ellipsoidal Harmonics. Theory and Applications*, 1st ed.; Cambridge University Press: Cambridge, UK, 2012
18. Dassios, G. Second order low frequency scattering by the soft ellipsoid. *Siam J. Appl. Math.* **1980**, *38*, 373–381. [CrossRef]

19. Charalambopoulos, A.; Dassios, G. Scattering of a spherical wave by a small ellipsoid. *IMA J. Appl. Math.* **1999**, *62*, 117–136. [CrossRef]
20. Lebedev, N.N. *Special Functions and Their Applications*, 1st ed.; Prentice Hall: Hoboken, NJ, USA, 1965.
21. Charalambopoulos, A. An analytic algorithm for shape reconstruction from low-frequency moments. *J. Math. Phys.* **2011**, *52*, 32. [CrossRef]
22. Paris, F.; Canas, J. *Boundary Element Method—Foundations and Applications*; Oxford University Press: Oxford, UK, 1997.
23. Polyzos, D.; Tsinopoulos, S.V.; Beskos, D.E. Static and dynamic boundary element analysis in incompressible linear elasticity. *Eur. J. Mech. A/Solids* **1998**, *17*, 515–536. [CrossRef]
24. Charalambopoulos, A.; Dassios, G.; Hadjinikolaou, M. An analytic solution for low-frequency scattering by two soft spheres. *Siam J. Appl. Math* **1998**, *58*, 370–386. [CrossRef]